the plant journal

SEB Society for Experimental Biology

The Plant Journal (2017) **92,** 1182–1201 doi: 10.1111/tpj.13754

Arabidopsis lipid droplet-associated protein (LDAP) – interacting protein (LDIP) influences lipid droplet size and neutral lipid homeostasis in both leaves and seeds

Michal Pyc[1], Yingqi Cai[2], Satinder K. Gidda[1], Olga Yurchenko[3], Sunjung Park[3], Franziska K. Kretzschmar[4], Till Ischebeck[4], Oliver Valerius[5], Gerhard H. Braus[5], Kent D. Chapman[2], John M. Dyer[3,*] and Robert T. Mullen[1,*]

[1]*Department of Molecular and Cellular Biology, University of Guelph, Guelph, ON N1G 2W1, Canada,*

[2]*Department of Biological Sciences, Center for Plant Lipid Research, University of North Texas, Denton, TX 76203, USA,*

[3]*US Department of Agriculture, Agricultural Research Service, US Arid-Land Agricultural Research Center, Maricopa, AZ 85138, USA,*

[4]*Department of Plant Biochemistry, Albrecht-von-Haller-Institute for Plant Sciences, University of Goettingen, Justus-von-Liebig-Weg 11, 37007 Goettingen, Germany, and*

[5]*Department of Molecular Microbiology and Genetics, Institute for Microbiology and Genetics, University of Goettingen, Grisebachstrasse 8, 37077 Goettingen, Germany*

Received 10 August 2017; revised 25 September 2017; accepted 17 October 2017; published online 30 October 2017.
*For correspondence (e-mails john.dyer@ars.usda.gov; rtmullen@uoguelph.ca).

SUMMARY

Cytoplasmic lipid droplets (LDs) are found in all types of plant cells; they are derived from the endoplasmic reticulum and function as a repository for neutral lipids, as well as serving in lipid remodelling and signalling. However, the mechanisms underlying the formation, steady-state maintenance and turnover of plant LDs, particularly in non-seed tissues, are relatively unknown. Previously, we showed that the LD-associated proteins (LDAPs) are a family of plant-specific, LD surface-associated coat proteins that are required for proper biogenesis of LDs and neutral lipid homeostasis in vegetative tissues. Here, we screened a yeast two-hybrid library using the Arabidopsis LDAP3 isoform as 'bait' in an effort to identify other novel LD protein constituents. One of the candidate LDAP3-interacting proteins was Arabidopsis At5g16550, which is a plant-specific protein of unknown function that we termed LDIP (LDAP-interacting protein). Using a combination of biochemical and cellular approaches, we show that LDIP targets specifically to the LD surface, contains a discrete amphipathic α-helical targeting sequence, and participates in both homotypic and heterotypic associations with itself and LDAP3, respectively. Analysis of *LDIP* T-DNA knockdown and knockout mutants showed a decrease in LD abundance and an increase in variability of LD size in leaves, with concomitant increases in total neutral lipid content. Similar phenotypes were observed in plant seeds, which showed enlarged LDs and increases in total amounts of seed oil. Collectively, these data identify LDIP as a new player in LD biology that modulates both LD size and cellular neutral lipid homeostasis in both leaves and seeds.

Keywords: *Arabidopsis thaliana*, endoplasmic reticulum, LDAP, LDIP, lipid droplet, neutral lipids, organelle biogenesis, protein targeting.

INTRODUCTION

Cytoplasmic lipid droplets (LDs) are evolutionarily conserved organelles that compartmentalize storage lipids such as sterol esters and triacylglycerols (TAGs). Structurally, LDs consist of a neutral lipid core uniquely enclosed by a single phospholipid monolayer and coated with a diverse array of 'coat' proteins that either bind the LD surface directly or embed themselves into the monolayer (Murphy, 2012). The formation of LDs occurs *de novo* between the leaflets of the endoplasmic reticulum (ER) membrane in what is considered to be a complex, multistep process (Thiam and Forêt, 2016; Barneda and Christian, 2017; Chen and Goodman, 2017). Briefly, the synthesis and accumulation of TAG within the ER bilayer serves to initiate the core of a nascent LD, which is thought to occur at specialized sites (subdomains) of the ER. Then, through the concerted action of various ER membrane and

soluble cytoplasmic proteins that are recruited to the growing LD, along with the continued addition of TAG to the LD core and coordinated changes in the phospholipid composition of the LD monolayer, the LD matures and eventually detaches from the ER into the cytoplasm; in some instances it can stay permanently connected with the ER. While the mechanistic details underlying these events have begun to be elucidated, albeit less so for plant LDs (Chapman *et al.*, 2012; Pyc *et al.*, 2017), the general process of LD biogenesis appears to be relatively well conserved among evolutionarily diverse species (Thiam and Beller, 2017). There is also a growing appreciation that LDs, long considered to be static fat depots that merely serve as energy reservoirs, are far more dynamic in nature and function in a multitude of cellular and physiological processes (Welte and Gould, 2017).

In plants, ER-derived cytoplasmic LDs have mostly been studied in pollen and oilseeds; in the latter they are responsible for providing the required carbon and energy for pre-photosynthetic development of the germinated seedling. In seeds, oleosins are the predominant LD coat proteins and play a role in both the formation and stabilization of LDs during seed desiccation (Huang, 1996; Purkrtova *et al.*, 2008; Laibach *et al.*, 2015; Pyc *et al.*, 2017). However, LDs are present in virtually all plant cell types, many of which are devoid of oleosins. This observation has recently led to increased efforts to identify LD proteins in non-seed tissues/organs (Gidda *et al.*, 2013; Horn *et al.*, 2013; Davidi *et al.*, 2015; Huang and Huang, 2016; Brocard *et al.*, 2017), as well as to probe the function of LDs in cell types that do not specialize in fat storage (Shimada *et al.*, 2014; Gidda *et al.*, 2016; McLachlan *et al.*, 2016; Zhang *et al.*, 2016).

Lipid droplet-associated proteins (LDAPs) are among the proteins implicated recently in LD biology in non-seed tissues (Horn *et al.*, 2013). These are considered to be functionally similar to the small rubber particle proteins (SRPPs) involved in the formation and stabilization of polyisoprenoid-containing LDs in rubber-producing plants (Berthelot *et al.*, 2016). In Arabidopsis, LDAPs constitute a three-member family (termed LDAP1–3) of ubiquitously expressed LD coat proteins that are critical for the proper maintenance and regulation of LDs during various developmental and stress-related processes (Gidda *et al.*, 2016). For instance, the abundance of LDs in leaves varies throughout the diurnal cycle, and this process is regulated, at least in part, by LDAP. Further, despite similarities of the LDAPs in terms of their ability to modulate LD abundance, exposure of plants to heat or cold stress results in the differential induction of *LDAP* genes, and analysis of loss-of-function mutants confirmed that specific *LDAP*s are required for the proliferation of LDs under different stress conditions (Gidda *et al.*, 2016). Consistent with these results, the LDAPs have also been implicated in drought stress response as well as in overall plant growth and development (Kim *et al.*, 2010, 2016; Seo *et al.*, 2010; Brocard *et al.*, 2017), suggesting broader roles for LDAPs and LDs in plant physiological processes and stress adaptations.

Given that LDAPs are involved in multiple aspects of LD biology, and that LD coat proteins are known to function in general as part of highly regulated protein–protein interaction networks in other organisms (Tsai *et al.*, 2015; Kolkhof *et al.*, 2017), we employed Arabidopsis LDAP3 as 'bait' in a yeast two-hybrid (Y2H) assay screen to identify new proteins involved in biogenesis and/or function of plant LDs. We chose LDAP3 as the specific 'bait' since it is the most highly and ubiquitously expressed *LDAP* gene in Arabidopsis, including in seeds (Gidda *et al.*, 2016). One of the interacting proteins identified was Arabidopsis At5g16550, which, depending on the database, is annotated to be of unknown function or a putative voltage-dependent L-type calcium channel subunit, but has regions of similarity to the mycobacterial membrane protein large (MmpL) family of proteins and the promethin protein in mammals, both of which are known to be involved in various aspects of lipid metabolism (Yu *et al.*, 2004; Viljoen *et al.*, 2017). Here, we provide evidence that At5g16550, which we refer to hereafter as LDIP (LDAP-interacting protein), is a *bona fide* constituent of LDs in plant cells which physically interacts with LDAP3 on the LD surface; furthermore, it is also found on oleosin-containing LDs derived from germinated Arabidopsis seedlings. Analysis of two independent mutants with disruptions in *LDIP* gene expression revealed pronounced changes in LD abundance and morphology in plant leaves, with a reduction in the number of LDs and increases in LD size and variability, as well as increases in the total neutral lipid content in leaves. Similar changes in LD morphology and neutral lipid content were observed in *LDIP* mutant seeds. Together, these and other results identify LDIP as a new component of the cellular machinery involved in the modulation of LD abundance and size in plants; further, this proper compartmentalization is required for the maintenance of neutral lipid homeostasis in both leaves and seeds.

RESULTS

Identification of LDIP as a new LD protein in plant cells

The use of LDAP3 as 'bait' in a Y2H screen against a normalized Arabidopsis cDNA library resulted in identification of nine candidate interacting proteins (Table 1). To determine whether any of these proteins represented a new LD protein constituent, each was fused to the C-terminus of green fluorescent protein (GFP) then transiently expressed via *Agrobacterium tumefaciens* infiltration into *Nicotiana benthamiana* tobacco leaves and visualized using confocal laser-scanning microscopy (CLSM). As shown in Figure S1

Table 1 List of candidate LDAP3-interacting proteins identified by yeast two-hybrid (Y2H) analysis

AGI no.[a]	Name	Y2H association[b]	Description[c]	SUBA localization[d]	GFP localization[e]
At2g39990	EIF2	Strong (1)	Translation initiation factor eIF2 p47 subunit homologue	Nucleus, cytoplasm	Cytoplasm
At3g21190	MSR1	Strong (2)	O-fucosyltransferase family protein	Golgi	Golgi
At4g08320	TPR8	Strong (1)	Tetratricopeptide repeat (TPR)-like superfamily protein	Nucleus	Cytoplasm
At1g55190	PRA7	Weak (1)	PRA1 (prenylated rab acceptor) family protein	Vacuole	ER
At1g79690	NUDT3	Weak (1)	Nudix hydrolase homolog 3	Cytoplasm	Cytoplasm
At5g13420	TRA2	Weak (2)	Aldolase-type triosephosphate isomerase (TIM barrel) family protein	Plastid	Cytoplasm
At5g16550	LDIP[f]	Weak (6)	Unknown protein; putative voltage-dependent L-type calcium channel subunit	ER	LD
At5g17920	ATMS1	Weak (1)	Cobalamin-independent synthase family protein	Cytoplasm	Cytoplasm
At5g24420	PGL5	Weak (1)	6-phosphogluconolactonase 5	Cytoplasm	Cytoplasm

[a]The Arabidopsis gene identifier (AGI) number represents the systematic designation given to each locus, gene and its corresponding protein product(s) by The Arabidopsis Information Resource (TAIR; http://www.arabidopsis.org).
[b]Strong and weak interacting 'prey' proteins identified in the Y2H screen based on the relative growth of yeast on selective media. The number of times that each 'prey' protein was identified in the screen is indicated in parentheses.
[c]Information on protein function and/or homology summarized from TAIR, Araport (https://www.araport.org) and SUBA (Subcellular Localization Database for Arabidopsis Proteins; http://suba.live/).
[d]Protein intracellular (consensus) localization based on SUBA.
[e]Intracellular localization of C-terminal GFP-tagged fusion protein in *Agrobacterium*-infiltrated tobacco leaf epidermal cells (refer to Figure S1).
[f]Named LDIP (lipid drop-associated protein-interacting protein) in this study.

in the Supporting Information, GFP-At5g16550 (GFP-LDIP) was the only fusion protein that localized to Nile red-stained LDs. All other candidate proteins displayed exclusively cytoplasmic localizations, except for GFP-At1g55190 (i.e. PRA7) and GFP-At3g21190 (i.e. MSR1), which were localized to the ER and Golgi, respectively (Figure S1). As shown Figure 1(a), high-magnification images of LDIP appended to a monomeric version of GFP (mGFP-LDIP) in tobacco epidermal cells revealed distinct toroidal shapes that encircled the Nile red-stained LD cores, indicating that mGFP-LDIP is localized to the surface of the LD (Figure 1a). Localization to LDs was also observed in BODIPY-stained epidermal and mesophyll cells of tobacco leaves when LDIP was fused to the Cherry fluorescent protein (Cherry-LDIP) (Figure 1a). Similarly, Cherry- and mGFP-tagged LDIP co-localized with the LD marker proteins oleosin-mGFP and LDAP3-Cherry (Figure 1a).

To confirm that LDIP represents a *bona fide* LD protein in plants, 2-day-old, germinated Arabidopsis seedlings were harvested and homogenized and then LDs were purified by differential centrifugation. The resulting total cell and isolated LD fractions were then analysed using Western blotting or mass spectrometry (MS)-based proteomics. Antibodies were raised to a unique peptide sequence in Arabidopsis LDIP (see Experimental Procedures for details) and the quality of antibodies was verified by Western blot analysis of proteins extracted from tobacco leaves transiently expressing either Cherry-tagged or non-tagged LDIP. As shown in Figure 1(b), bands of the expected sizes were observed for both Cherry-LDIP (about 55.4 kDa) and native LDIP (about 26.6 kDa) proteins. A band of the expected size for native LDIP was also observed in total protein extracts derived from Arabidopsis seedlings, and this protein was strongly enriched in the purified LD fraction (Figure 1b). Moreover, the presence of LDIP in these fractions was confirmed by label-free quantitative proteomics, which showed that while LDIP occurs at relatively low abundance it was clearly enriched in the purified LD fraction, along with several other known LD marker proteins (Figure 1c). Marker proteins for various other subcellular compartments, however, were not enriched in the LD fraction (Figure 1c) (refer to Tables S1 and S2 for all the proteomics data obtained). Taken together with the results above, these data indicate that LDIP represents a new LD protein in plants.

LDIP is a plant-specific protein that is constitutively expressed in Arabidopsis

To gain insight to the evolutionary history of LDIP and the distribution of homologues within the plant kingdom, phylogenetic analyses were performed comparing the deduced polypeptide sequence for Arabidopsis LDIP with other protein sequences encoded in extant genomic databases. The results indicated that LDIP is a plant-specific protein with closely related homologues found throughout most of the plant kingdom, including in bryophytes, gymnosperms, monocots and dicots (Figure 2a). However, no homologues were detected in algal species or in yeasts

(a)

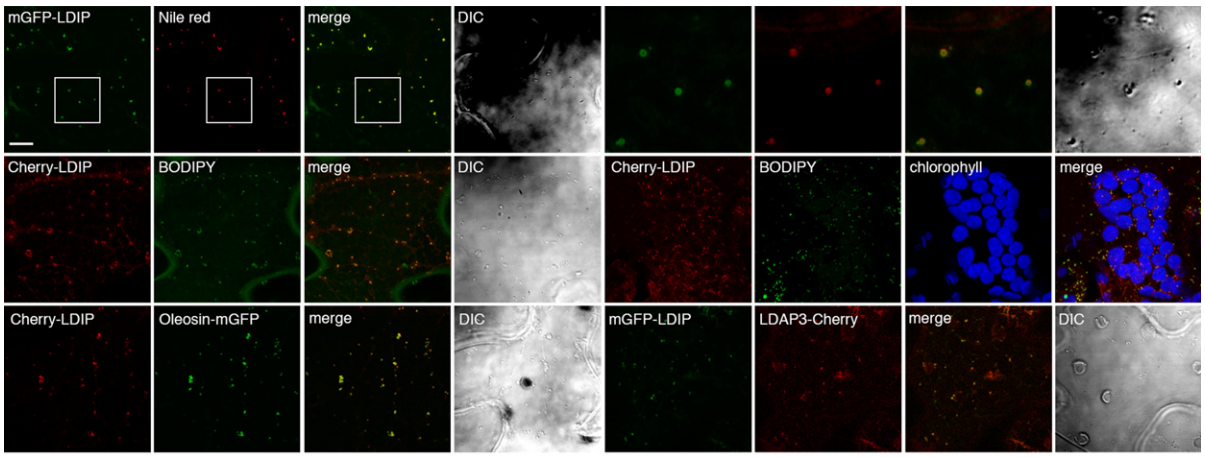

(b)

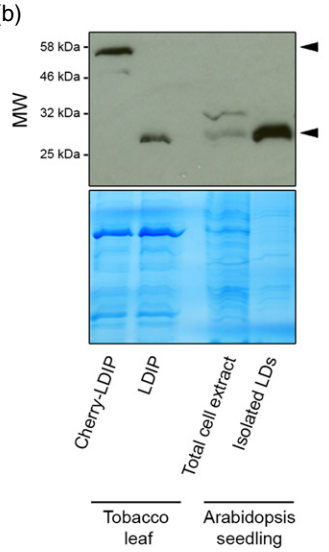

(c)

AGI No.	Name	Enrichment factor	iBAQ	
			LD	Total
At5g16500	LDIP	54.7	0.016±0.014	0.0003±0.0005
Known LD proteins				
At3g05500	LDAP3	44.4	0.054±0.042	0.0012±0.0021
At4g25140	Oleosin 1	15.0	174.1±68.3	11.6±5.1
At5g51210	Oleosin 3	11.3	4.16±0.62	0.37±0.43
At3g27660	Oleosin 4	9.4	92.8±28.7	9.9±4.0
At5g40420	Oleosin 2	9.1	104.9±10.4	11.5±4.4
At4g10020	Hydroxysteroid dehydrogenase 5	9.0	0.42±0.11	0.05±0.04
At2g25890	Oleosin family member	8.5	2.75±0.32	0.32±0.22
At5g55420	Caleosin 2	8.2	3.95±1.23	0.48±0.19
At3g18570	Oleosin family member	8.2	6.22±1.15	0.76±0.65
At2g47780	LDAP2	8.1	2.07±1.14	0.26±0.05
At3g01570	Oleosin family member	7.6	112.65±23.90	14.91±6.34
At4g26740	Caleosin 1	7.2	5.75±0.78	0.79±0.14
At5g50700	Hydroxysteroid dehydrogenase 1	5.5	19.09±5.05	3.47±1.35
At3g01420	α-Dioxygenase1	4.8	0.008±0.006	0.0016±0.0023
At1g48990	Oleosin family member	3.6	1.24±0.83	0.34±0.32
At1g67360	LDAP1	NC	0.004±0.006	0.0000±0.0000
Known non-LD organelle marker proteins				
At4g28520	12S seed storage protein (Protein body)	0.778	136.3+51.8	175.2+45.1
At5g61790	Calnexin homolog 1 (ER membrane)	0.607	0.142+0.128	0.234+0.057
At1g09210	Calreticulin 2 (ER lumen)	0.255	0.018+0.015	0.074+0.038
At3g16240	Aquaporin TIP2-1 (Tonoplast)	0.207	0.205+0.146	0.99+1.00
At3g16420	PYK10-binding protein 1 (ER body)	0.190	2.133+1.384	11.21+3.02
At3g08580	ADP/ATP carrier protein 1 (Mitochondrion)	0.124	0.391+0.237	3.14+0.34
At3g04120	GADPH C subunit 1 (Cytoplasml)	0.035	0.418+0.261	11.78+1.45
At3g21720	Isocitrate lyase (Peroxisome)	0.029	0.190+0.120	6.51+3.42
At1g53240	Malate dehydrogenase 1 (Mitochondrion)	0.023	0.134+0.109	5.80+0.67
AtCg00490	Rubisco large chain (Plastid)	0.021	0.121+0.059	5.81+4.13
At1g04410	Malate dehydrogenase 1 (Cytoplasm)	0.007	0.026+0.009	3.85+1.30

Figure 1. Localization of lipid drop-associated protein (LDAP)-interacting protein (LDIP) in plant cells.
(a) Representative confocal laser-scanning microscopy images of tobacco leaf cells transiently (co)expressing (as indicated by labels) mGFP- or Cherry-tagged LDIP and either oleosin-mGFP or LDAP3-Cherry, or stained with the neutral lipid-selective dye Nile red or BODIPY. For each set of images the corresponding merged and differential interference contrast (DIC) images or the corresponding image of endogenous chlorophyll autofluorescence of the mesophyll cells (middle row, right set of images) is shown; all other sets of images in (a) are of leaf epidermal cells. Also, images of the mesophyll cells are a *z*-stack series, whereas all other images shown are single (individual) optical sections. Boxes (top row) represent the portion of the cell shown at higher magnification to the right, revealing the localization of mGFP-At5g16550 (LDIP) to the surface of several, individual Nile red-stained lipid droplets (LDs). Bar = 20 μm.
(b) Western blot analysis of total cell protein extracts from tobacco leaves transiently transformed (via *Agrobacterium* infiltration) with Cherry-tagged LDIP or non-tagged LDIP and total cell protein and isolated LD protein extracts from 2-day-old Arabidopsis seedlings. The relative positions of expressed Cherry-LDIP or non-tagged LDIP in tobacco or native (endogenous) LDIP in Arabidopsis are indicated with arrowheads. Positions of molecular mass markers are also indicated. Also shown is the corresponding Coomassie-stained gel of the same protein extracts that were analysed by Western blotting with anti-LDIP IgGs.
(c) Identification of LDIP in the label-free LD proteome of Arabidopsis seedlings. The identical 2-day-old Arabidopsis seedling total cell protein and LD fractions used in (b), as well as two additional replicates ($n = 3$), were subjected to LC-MS/MS-based shotgun proteomic analysis. Protein levels were calculated using the intensity-based quantification (iBAQ) label-free algorithm. The values were normalized, setting the sum of all abundances to 1000. Depicted are iBAQ values for LDIP and selected known LD and non-LD proteins (AGI numbers and protein names were obtained from the TAIR database) as the mean of the total values of three separate samples (±SD). Also depicted is the corresponding LD/total cell enrichment ratio as determined for each protein. See Table S1 and S2 for the iBAQ values and enrichment ratios for all proteins identified in all samples.

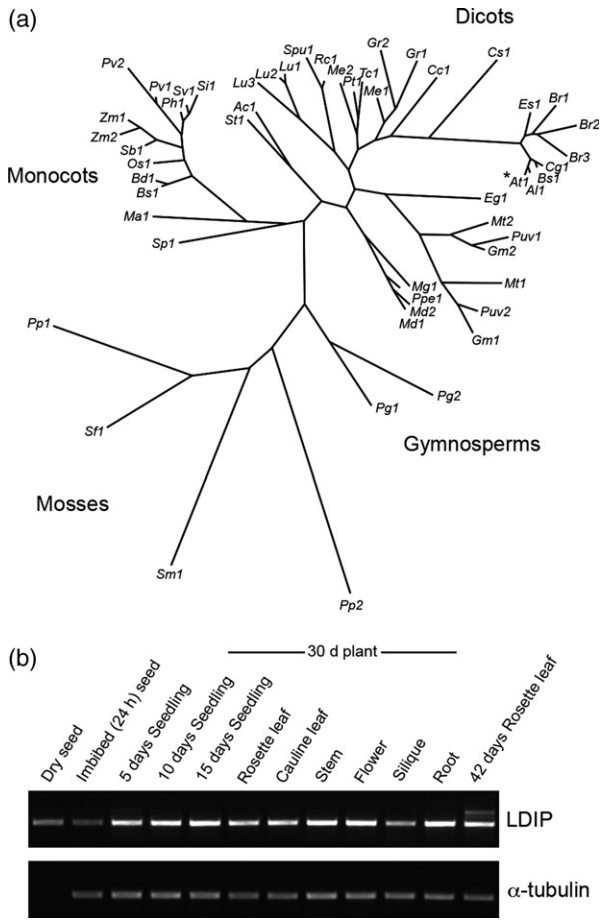

Figure 2. Phylogenetic analysis of lipid drop-associated protein-interacting proteins (LDIPs) and expression of *LDIP* in Arabidopsis.
(a) Phylogenetic tree depicting the evolutionary relationship of LDIP-like proteins across various plant species, including those found in distinct clades corresponding (as indicated) to mosses, gymnosperms, monocots and dicots. Each protein is labelled with the respective genus and species, and numerically, including those that exist as multiple homologues in some species. Arabidopsis LDIP (At1) is indicated with an asterisk.
(b) RT-PCR analysis of *LDIP* gene expression in various organs and developmental stages in Arabidopsis, as indicated by labels. α-tubulin served as an endogenous control.

and metazoans. In Arabidopsis, LDIP is present as a single copy, whereas two or sometimes three homologues exist in some other plant species (Figure 2a), reflecting whole-genome duplication events known to have occurred during plant evolution (Paterson *et al.*, 2010).

To determine the expression pattern of *LDIP* in Arabidopsis, reverse transcription–polymerase chain reaction (RT-PCR) assays were used to assess the transcript levels in mRNA derived from various organs at different developmental stages. As shown in Figure 2(b), *LDIP* is expressed at comparable levels in all organs examined during plant growth and development, including in mature dry seeds. This expression pattern is similar to that of the Arabidopsis *LDAP* genes, especially *LDAP2* and *LDAP3,* which are also constitutively expressed, including in seeds (Gidda *et al.*, 2016). However, the pattern is different from certain other LD-specific proteins, such as oleosins, which are expressed predominantly in seeds and pollen (Kim *et al.*, 2002; Ischebeck, 2016). Taken together, these observations suggest that LDIP is probably involved in LD-related processes throughout the entire plant life cycle, including in both leaves and seeds.

LDIP contains an amphipathic α-helix-type LD targeting signal

To further analyse the relationship of LDIP with LDs, we next investigated whether the protein contains a discrete LD targeting sequence. To help guide the design of these experiments, we analysed the Arabidopsis LDIP sequence along with several phylogenetically diverse homologues using both polypeptide sequence alignments and hydropathy profile analyses (Figure 3a, b). The results indicated that each of the proteins has three fairly distinct regions: (i) an N-terminal section (amino acid residues 1–106 in Arabidopsis LDIP) that possess relatively little sequence similarity/identity and is hydrophilic overall, with the exception of a mildly hydrophobic segment (residues 50–65 in Arabidopsis LDIP); (ii) a middle section (residues 107–211 in Arabidopsis LDIP) consisting of a more highly conserved and strongly hydrophobic sequence, including several predicted transmembrane-spanning domains (Figure 3b); and (iii) a C-terminal section (residues 212–249 in Arabidopsis LDIP) that, similar to the N-terminal region, is a less conserved and primarily hydrophilic sequence. Notably, BLASTP analysis with Arabidopsis LDIP or its homologues revealed little sequence conservation with any other proteins, although the middle hydrophobic region possesses some similarity to domains present in the MmpL family and the mammalian promethin protein (Yu *et al.*, 2004; Viljoen *et al.*, 2017).

Based on this information, we constructed a series of truncation mutants of Arabidopsis LDIP that were subsequently fused to the Cherry fluorescent protein, and then transiently expressed the proteins in tobacco epidermal cells to assess their subcellular localization. As shown in Figure 3(c), Cherry-LDIP$^{1–106}$, which lacks the C-terminal and hydrophobic middle regions of the protein, localized to LDs in a manner similar to full-length Arabidopsis LDIP (Cherry-LDIP), indicating that the N-terminal region of the protein (i.e. residues 1–106) is sufficient for targeting LDs. Deletion of this region confirmed it was also necessary for LD targeting, since Cherry-LDIP$^{211–249}$, consisting of the C-terminal section alone, and Cherry-LDIP$^{107–249}$, consisting of the C-terminal and hydrophobic middle sections together, mislocalized to the cytoplasm and ER, respectively (Figures 3c and S2).

To gain additional insight into the nature of the N-terminal LD targeting signal in Arabidopsis LDIP, we analysed

the 1–106 polypeptide sequence for possible structural features including hydrophobic domains and amphipathic α-helices, which are known to serve as LD targeting signals in mammals and yeast (Kory *et al.*, 2016; Bersuker and Olzmann, 2017). This analysis revealed a possible amphipathic α-helix (Figure 3d) that corresponded to the moderately hydrophobic sequence present in the N-terminal region (residues 50–65, see Figure 3b). The amphipathic characteristics of this hydrophobic region were relatively well conserved in other LDIP homologues (Figures 3b and S3). Moreover, analysis of the full-length Arabidopsis LDIP protein sequence using the structural homology-modelling tool available at SWISS-MODEL showed that while there were no sequences that were sufficiently similar for modelling the entire 3D structure of the protein, a significant portion of region 1–106 (residues 32–115; italicized in Figure 3a) matched several known protein structures available in the database. Development of a homology model for this N-terminal region of Arabidopsis LDIP revealed five secondary structures (Figure 3e; see also Figure 3b), the second of which was an α-helix that corresponded almost perfectly to the region predicted to form the amphipathic α-helix (Figure 3d, e).

To help determine the importance of the predicted amphipathic α-helix sequence for LDIP targeting to LDs, we generated two mutant versions of Cherry-LDIP$^{1–106}$: (i) Cherry-LDIP$^{1–106\ Mut1}$, whereby amino acids 50–65 in LDIP comprising the hydrophobic sequence and the majority of the amphipathic helix (Figure 3d), were deleted; and (ii) Cherry-LDIP$^{1–106\ Mut2}$, whereby the two isoleucine residues at positions 55 and 59 located near the centre of the hydrophobic face of the amphipathic helix (refer to Figure 3d) were replaced with hydrophilic glutamic acids. As shown in Figure 3(f), both mutant fusion proteins, in contrast to LD-localized, wild-type Cherry-LDIP$^{1–106}$ (Figures 3c and S2), mislocalized to the cytoplasm in tobacco leaf epidermal cells, suggesting that LDIP contains an amphipathic-helix-type LD targeting signal similar to that found in other proteins that target to LDs via the cytoplasm.

LDIP interacts with itself and LDAP3 in yeast and plant cells

We next performed a more detailed assessment of the physical interactions between Arabidopsis LDIP and LDAP3. As shown in Figure 4(a), co-expression of full-length LDIP and LDAP3 as 'bait' and 'prey' fusion proteins, respectively, in the Y2H system resulted in cell growth under selective conditions, as expected (see Table 1). Similar results were observed when the orientation of proteins was switched between the bait and prey vectors (Figure S4), and also when LDIP was paired with itself (Figure 4a). Cell growth was not observed, however, when LDIP was co-expressed with a mutant version of LDAP3 lacking its C-terminal 100 amino acids (i.e. LDAP3ΔC100) (Figure 4a), which disrupts the association of LDAP3 with LDs in plant cells (Gidda *et al.*, 2016). Cell growth was also abolished when each protein was expressed with the corresponding empty vector control, as expected (Figures 4a and S4). Western blotting was used to confirm the presence of proteins in all yeast strains tested (Figure S5). Taken together, these data indicate that LDIP and LDAP3 interact in yeast cells, and that LDIP is capable of homotypic association.

To characterize the interaction of Arabidopsis LDIP and LDAP3 *in planta*, the proteins were fused to the C-terminal half of cyan fluorescent protein (cCFP) and the N-terminal half of the yellow fluorescent protein Venus, respectively, which by themselves are not fluorescent. The resulting fusion proteins were then transiently expressed in tobacco leaf epidermal cells, and protein–protein interactions assessed based on bimolecular fluorescence complementation (BiFC). Given that BiFC can result from false positive interactions (i.e. the two halves of the fluorescent proteins can assemble if the proteins being tested are merely in close proximity to one another and are not necessarily interacting (see Stefano *et al.* (2015) and Xing *et al.* (2016)), two experiments were performed in parallel: tobacco leaves were co-infiltrated with either cCFP-LDIP and nVenus-LDAP3 or cCFP-LDIP and nVenus-LDAP3ΔC100, the latter serving as a negative control since LDAP3ΔC100 does not target to LDs (Gidda *et al.*, 2016). In addition, cells were transformed with Cherry-Perox, which is a marker protein that targets to peroxisomes (Ching *et al.*, 2012) and was used to identify transformed cells, regardless of whether a BiFC signal was present or not. As shown in Figure 4(b) and quantified in Figure 4(c), co-expression of cCFP-LDIP and nVenus-LDAP3 resulted in numerous BiFC puncta, and staining of these cells with monodansylpentane (MDH), a blue-fluorescent neutral lipid dye (Yang *et al.*, 2012), confirmed that the puncta were LDs (Figure 4d). Further, the LDs were aggregated in a manner similar to the LDs in cells transformed with GFP-LDIP (compare the images in Figures 4d and S1). By contrast, co-expression of cCFP-LDIP and nVenus-LDAP3ΔC100 resulted in significantly fewer BiFC puncta compared with co-expression of full-length proteins (Figure 4b, c). The decrease in fluorescence of the negative control was not due to differences in transgene expression, since RT-PCR analysis confirmed similar levels of gene transcripts in both experiments (Figure S6).

Biochemical evidence in support of interaction of Arabidopsis LDIP and LDAP was obtained using a GFP-based affinity-capture method, whereby GFP-LDIP was first transiently expressed in tobacco leaves, then leaves were homogenized, proteins were solubilized in detergent and GFP-LDIP and interacting proteins were isolated using the GFP trap system (see Experimental Procedures for details). Co-purifying proteins were then identified using MS and peptide mass fingerprinting, which identified a number of

different LD proteins, including endogenous tobacco LDAPs and SEIPINs, as well as a tobacco homologue of Arabidopsis LDIP (Figure 4e). These results were consistent with Y2H analyses (Figure 4a), which showed both homotypic and heterotypic associations between LDIP and LDAP3. Furthermore, co-expression in tobacco leaves of GFP-LDIP with the Arabidopsis LEAFY COTYLEDON2 (LEC2) transcription factor, which induces genes for seed oil-like synthesis in leaves (Santos Mendoza *et al.*, 2005; Vanhercke *et al.*, 2017), resulted in co-purification of GFP-LDIP with several tobacco oleosins (Figure 4e), which are known to be induced by LEC2 when expressed in tobacco leaves (Kim *et al.*, 2013). None of these GFP-LDIP co-purifying proteins were identified when GFP was expressed on its own, with or without LEC2, in tobacco leaves (Figure 4e). Taken together, the data in Figure 4 provide strong evidence that LDIP and LDAPs interact at the surface of LDs, and furthermore that LDIP might have a role in conjunction with oleosins in plant seeds.

Disruption of *LDIP* alters LD morphology and abundance and increases neutral lipid content in leaves

To assess the function of LDIP in plants, we obtained two Arabidopsis *LDIP* T-DNA mutants from the Arabidopsis Biological Resource Center: SALK_084555, which contains a T-DNA inserted in the first intron, and SAIL_335_H11, which contains a tandem T-DNA inserted in the first exon (Figure S7). Each line was genotyped and advanced to homozygosity, then expression of *LDIP* was determined using RT-PCR. The results revealed that SALK_084555 was a knockdown (KD) mutant with reduced gene expression, while SAIL_335_H11 was a knockout (KO) mutant with no full-length transcripts detected (Figure S7).

Prior studies showed that the abundance of LDs in plant leaves changes throughout the diurnal cycle, with the highest number of LDs being present at the end of the dark period and the lowest numbers present at the end of the light period (Gidda *et al.*, 2016). To determine whether disruption of *LDIP* had any effects on LDs in leaves, wild-type (WT), KD and KO Arabidopsis lines were germinated on ½ MS plates, then 15-day-old seedlings were formaldehyde-fixed at either the end of the dark cycle or the end of the light cycle, followed by visualization of LDs with BODIPY staining and CLSM. As shown in Figure 5(a), disruption of *LDIP* resulted in progressive decreases in the abundance of LDs in both KD and KO lines compared with WT. This trend was observed at the end of both the dark and light periods (Figure 5a). Furthermore, disruption of *LDIP* led to progressively greater variation in LD size, with the appearance of several prominent 'supersized' LDs (i.e. LDs $\geq$2 μm diameter) in the KO leaves (Figure 5a). Indeed, these larger LDs were even more obvious, and clearly external to chloroplasts, in three-dimensional (3D) projections of surface-rendered, highly magnified CLSM images of cells (Figure 5a). Supersized LDs were also observed in older (i.e. 28 days

Figure 3. Identification of a lipid drop (LD)-targeting signal in lipid drop-associated protein-interacting protein (LDIP).
(a) Deduced polypeptide sequence alignment of Arabidopsis LDIP and selected homologues. Proteins are labelled with the respective genus and species and numerically, and correspond to the same labels as in Figure 2(a): *Arabidopsis thaliana* (At1), *Brassica rapa* (Br1), *Linum usitatissimum* (Lu3), *Panicum virgatum* (Pv1) and *Physcomitrella patens* (Pp1). Identical and similar amino acid residues in each protein are highlighted red and blue or green and indicated with asterisks and colons or periods, respectively. Numbers above each row of sequences represent specific amino acid residues. The Arabidopsis LDIP sequence (i.e. residues 32–115) that matches several known protein structures available in the SWISS-MODEL database is italicized and Roman numerals (I–V) and blue-shaded boxes correspond to the regions within this sequence that are predicted to form distinct secondary structures, as illustrated in (e). Also indicated for the Arabidopsis LDIP sequence is the region predicted to form an amphipathic α-helix (highlighted with a grey background; refer also to (d)), the overlapping, moderately hydrophobic sequence (residues 50–65, dashed underline; refer also to (b)), and the middle, strongly hydrophobic section of the protein (residues 107–211, solid underline; refer also to (b)).
(b) Hydropathy profiles of the deduced polypeptide sequence of Arabidopsis LDIP and selected homologues based on the TMHMM algorithm (Krogh *et al.*, 2001). Proteins shown are the same as those in (a). Note the strong hydrophobic sequence in the middle portion of each protein, as well as the relatively moderate hydrophobic sequence located in the vicinity of residue 50 in each protein, indicated with the arrowhead in Arabidopsis LDIP.
(c) Truncation analysis of Arabidopsis LDIP targeting to LDs in tobacco leaf cells. Representative confocal laser-scanning microscopy (CLSM) images of leaf epidermal cells transiently expressing (as indicated by labels) full-length or truncated versions Cherry-tagged LDIP along with the corresponding BODIPY-stained LDs, as well as the corresponding merged and differential interference contrast (DIC) images for each set of images. The numbers in the name of each mutant construct denote the amino acid residues in LDIP that were fused to Cherry fluorescent protein. Bar = 20 μm.
(d) Helical wheel projection of amino acid residues 48–65 in Arabidopsis LDIP. Shown is a portion of the Arabidopsis LDIP sequence (numbers represent specific amino acid residues) that includes the region predicted by HeliQuest to form an amphipathic α-helix (residues 48–65, highlighted with a grey background), which is also depicted in the α-helical wheel projection. Hydrophobic amino acid residues are coloured yellow, hydrophilic and charged residues are white and red or blue, respectively. The direction of the arrowhead in the helical wheel indicates the position of the hydrophobic face along the axis of the helix. The sequence predicted, based on SWISS-MODEL, to form an α-helix (residues 48–60, region II) is indicated by the blue-shaded box (refer also to (a) and (e)). The dashed line indicates the sequence (i.e. residues 50–65) that was deleted from Cherry-LDIP$^{1–106\ Mut1}$; asterisks indicate the two isoleucine residues i.e. I_{55} and I_{59}, that were replaced with glutamic acid residues in Cherry-LDIP$^{1–106\ Mut2}$ (refer to (f)).
(e) Structural modelling of Arabidopsis LDIP. BLAST alignments performed at the SWISS-MODEL website identified a region in Arabidopsis LDIP, i.e. residues 32–115 (refer to (a)) that was sufficiently similar to proteins with known 3D structures that allowed for homology-based modelling. Shown (left panel) are the relative positions of the five secondary structures (domains I–V) modelled in the 32–115 amino acid sequence of LDIP. Shown also (right panel) is a close-up image of the predicted α-helix, beginning at leucine 48 and ending at glycine 60 (i.e. domain II; refer also to (d)).
(f) Mutational analysis of the predicted amphipathic α-helix in Arabidopsis LDIP and effects on targeting to LDs in tobacco leaf cells. Representative CLSM images of leaf epidermal cells transiently expressing (as indicated by labels) modified versions of Cherry-tagged LDIP$^{1–106}$ (see text for details), along with the corresponding BODIPY-stained LDs, as well as the corresponding merged and DIC images. Bar = 20 μm.

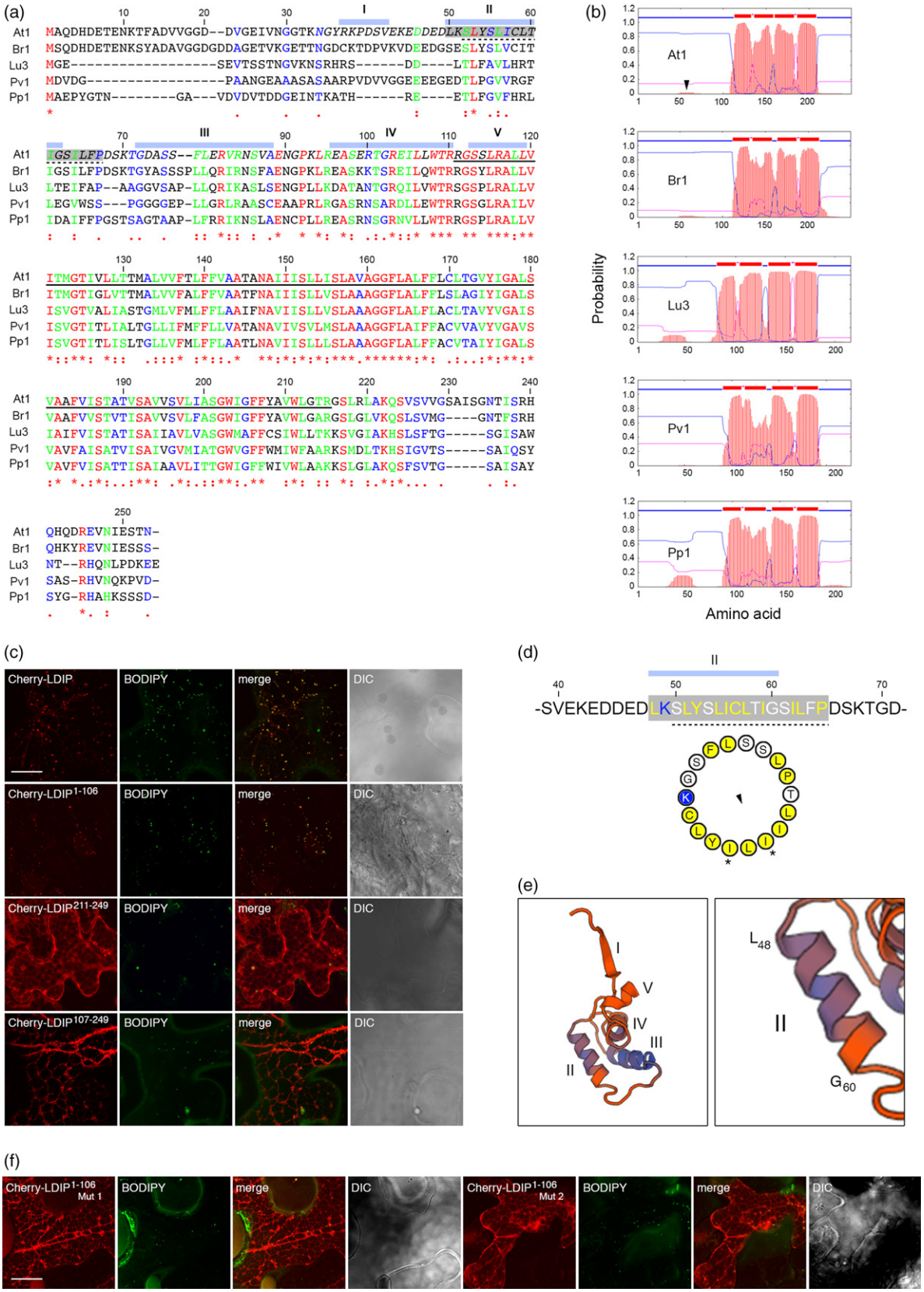

old) leaves of KO plants (Figure S8), indicating that this LD phenotype persists in other stages of plant growth and development.

To determine whether the changes in LD abundance and size in *LDIP* mutants affected leaf neutral lipid content, total lipids were extracted from 15-day-old seedlings at the end of both dark and light periods then neutral lipids and polar lipids were isolated by solid phase extraction, and fatty acid content determined using gas chromatography with flame ionization detection (GC/FID). As shown in Figure 5(b), neutral lipids were progressively increased in the KD and KO lines compared with WT, and these increases were apparent at the end of the dark period and, in the KO line, also at the end of the light period. Analysis of fatty acid composition revealed that these increases were due primarily to increases in linoleic (18:2) and linolenic (18:3) acids (Figure 5b), which are the most abundant fatty acids in leaf tissues (Li-Beisson *et al.*, 2013). By contrast, analysis of polar lipids showed no obvious changes in content or composition between WT, KD and KO lines (Figure 5c), suggesting that the effects of *LDIP* disruption were specific to neutral lipid homeostasis.

Taken together, these data indicate that loss of *LDIP* results in a decrease in LD abundance in plant leaves, an increase in the variability of LD size, the appearance of drastically enlarged LDs and changes in neutral lipid metabolism that result in increases in total neutral lipid content. Additional evidence that *LDIP* is responsible for these phenotypes comes from experiments where the KO line was backcrossed with WT, which resulted in normal LDs in F_1 plants, then a distribution of both normal and supersized LDs in a sorting F_2 population that was consistent with the phenotype being associated with a single Mendelian locus (Figure S9). Further, transformation of the KO line with either non-tagged LDIP or Cherry-LDIP resulted in complementation of the supersized LD phenotype in T_2 transgenic Arabidopsis lines, and Cherry-LDIP targeted to LDs in these plant lines, just as Cherry-LDIP did in WT plants when expressed under control of its native promoter (Figure S10).

Disruption of *LDIP* alters LD morphology and increases neutral lipid content in seeds

The observed expression of *LDIP* in seeds (Fig. 2), the co-enrichment of LDIP and oleosins in LDs isolated from germinated seedlings (Fig. 1c) and the co-immunoprecipitation of LDIP and oleosins from tobacco leaves transformed with LEC2 (Figure 4) prompted us to examine whether disruption of *LDIP* had any effects on LDs and/or neutral lipid content in seeds. As shown in Figure 6(a), CLSM analysis of mature dry seeds stained with BODIPY revealed the presence of noticeably enlarged LDs in cotyledons of KD and KO lines compared with WT. Analysis of lipids further revealed significant and progressive increases in the oil content of mature dry seeds in KD and KO lines relative to WT (Figure 6b), and these increases were due to increases in nearly all of the seed oil fatty acids (Figure 6c). The enlarged LDs and relatively higher neutral lipid content persisted throughout germination and seedling establishment, and notably more so in the KD line. While the reason for this more persistent phenotype in the KD line is currently unclear, RT-PCR analysis revealed that while the KO line did not produce any normal-length transcripts (Figure S7), it did possess transcripts that included a portion of the first exon of the *LDIP* sequence and the T-DNA insert sequence (Figure S11). Since translation of this latter RNA would generate a truncated version of the LDIP protein that also contains the LD targeting signal (Figure S11), perhaps this truncated protein contributed to changes in the LD proteome that affected the rate of breakdown of stored lipids during seedling establishment, different from that of the KD line. Regardless, by 4 days after the initiation of germination, the LDs and storage oil were largely degraded in both the KD and KO lines, as in the WT (Figure 6a–c). Taken together with the results presented above for leaves (Figure 5), these data clearly identify LDIP as a new and important player in neutral lipid metabolism and the modulation of LD abundance and size.

DISCUSSION

Identification of LDIP as an LD-localized, plant-specific protein

The identification and characterization of the Arabidopsis LDAPs has increased our understanding of plant LD biology as a whole and provided new insights into the roles of LDs, particularly in non-seed tissues (Gidda *et al.*, 2013, 2016; Horn *et al.*, 2013; Kim *et al.*, 2016). To identify additional proteins involved in LD biogenesis and/or function, we used LDAP3 as bait in a Y2H screen and identified nine candidate interacting proteins. Microscopic analysis of transiently expressed fluorescent protein-tagged versions of all nine proteins determined that only GFP-LDIP was targeted to LDs (Figure S1), although the non-LD localization of the others does not preclude them from having a role in LD-related processes (e.g. LDs might interact with other organelles or with proteins in the cytoplasm). LDIP was subsequently confirmed as a *bona fide* constituent of LDs using a variety of approaches, including co-localizations with oleosin or LDAP at LDs in tobacco leaves (Figure 1), isolation of LDs from germinating seedlings followed by Western blotting or proteomics, which showed clear enrichment of Arabidopsis LDIP in the LD fraction (Figure 1), and stable expression of Cherry-tagged LDIP in transgenic plants, which confirmed localization to LDs in Arabidopsis leaves and complemented the LDIP KO phenotype (Figure S10). Consistent with these data, LDIP was also identified as a

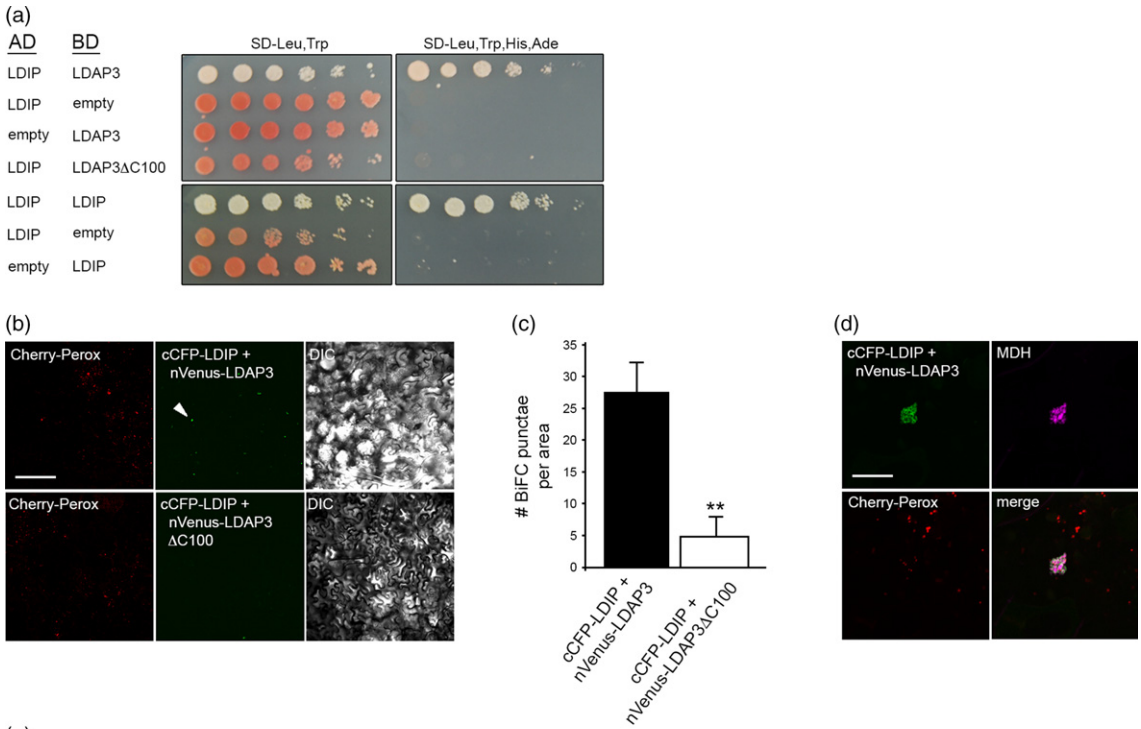

(e)

Accession No.	Normalized spectral count				Arabidopsis homolog(s)	
	GFP	GFP + LEC2	GFP-LDIP	GFP-LDIP + LEC2	AGI No.	Name
GFP	339.09	286.6	238.56	311.24	-	-
LDIP (GFP-LDIP)	0	0	115.93	143.03	-	-
NbS00061122g0002.1	0	0	11.50	2.70	At1g67360, At2g47780,At3g05500	LDAP1, LDAP2, LDAP3
NbS00011254g0004.1	0	0	0	11.70	At3g01570	Oleosin 5
NbS00033731g0004.1	0	0	9.58	15.29	At5g16550	LDIP
NbS00002723g0016.1	0	0	0	7.20	At5g51210	Oleosin 3
NbS00022037g0010.1	0	0	1.92	0.90	At5g16460, At1g29760, At2g34380	SEPIN1, SEIPIN2, SEPIN3
NbS00000657g0001.1	0	0	0	3.60	At3g18570	Oleosin family member
NbS00022599g0003,1	0	0	0	1.80	At4g25140	Oleosin 1
NbS00005370g0010.1	0	0	0	0.90	At4g10020	Hydroxysteroid dehydrogenase 5

Figure 4. Interaction of lipid drop-associated protein (LDAP)-interacting protein (LDIP) and LDAP3 in yeast and plant cells.
(a) Interaction of LDIP with itself and LDAP3 in the yeast two-hybrid (Y2H) assay. Yeast strains were co-transformed with the indicated pairs of GAL4-activating domain (AD) and GAL4-binding domain (BD) fusion proteins or the corresponding 'empty' AD or BD plasmids, serving as negative controls. Serial dilutions of cells were spotted onto plates containing either low-stringency [synthetic dextrose media lacking leucine and tryptophan (SD-Leu, Trp)] or high-stringency (SD-Leu, Trp, His, Ade) selection, the latter of which requires protein–protein interactions for yeast growth.
(b) Interaction of LDIP and LDAP3 in the bimolecular fluorescence complementation (BiFC) assay in tobacco leaf cells. Representative confocal laser-scanning microscopy (CLSM) images of leaf epidermal cells transiently (triple) transformed (via *Agrobacterium* infiltration) with Cherry-Perox, which serves as a transformation control, cCFP-LDIP, and either nVenus-tagged full-length LDAP3 or LDAP3 lacking its C-terminal 100 amino acid residues (nVenus-LDAP3ΔC100). Also shown are the corresponding differential interference contrast images. Note the relative abundance of the BiFC puncta (arrowhead), which are aggregates of LDs (refer to (d)), in areas of cells transformed (based on Cherry-Perox fluorescence) with cCFP-LDIP and nVenus-LDAP3, compared with cells transformed with cCFP-LDIP and nVenus-LDAP3ΔC100; refer also to (c). Bar = 20 μm.
(c) Quantification of BiFC assays with LDIP and LDAP3 in tobacco leaf cells. Results from at least 20 areas of transformed epidermal leaf cells, similar to those shown in (a), were analysed from three independent experiments, and the mean number of BiFC puncta per area (±SD) are plotted in the graph on the right. Asterisks indicate significant difference at $P \leq 0.01$ determined by Student's *t*-test.
(d) LDIP and LDAP3 interact at LDs in the BiFC assay in tobacco leaf cells. Representative CLSM images of an individual BiFC puncta in a cCFP-LDIP and nVenus-LDAP3-transformed leaf epidermal cell (refer to the example shown at lower magnification and indicated with an arrowhead in (b)) and the corresponding staining of LDs with monodansylpentane (MDH; false coloured magenta). Also shown is the corresponding image of co-expressed Cherry-Perox at peroxisomes, as well as the merged image. The aggregation of LDs is presumably due to organelle 'zippering' caused by the dimerization of the reconstituted fluorescent protein, similar to that observed in GFP-LDIP-transformed cells (Figure S1). Bar = 5 μm.
(e) Pull-down of LDAP and LDIP in tobacco leaf cells. Listed are selected MS-identified *N. benthamiana* LD proteins that co-immunoprecipitated with expressed GFP-LDIP or GFP alone, with or without co-expressed LEC2, in total protein extracts obtained from *Agrobacterium*-infiltrated tobacco leaves. Accession numbers of *N. benthamiana* proteins were obtained from the *N. benthamiana* genome, available at the Sol Genomics Network (http://www.solgenomics.net). AGI numbers and protein names of Arabidopsis homologues were obtained from TAIR database. The quantities (normalized spectra counts) of the co-purifying proteins were analysed using Scaffold software. Spectra counts of each protein were normalized to the average of the sums of all MS samples in the experiment.

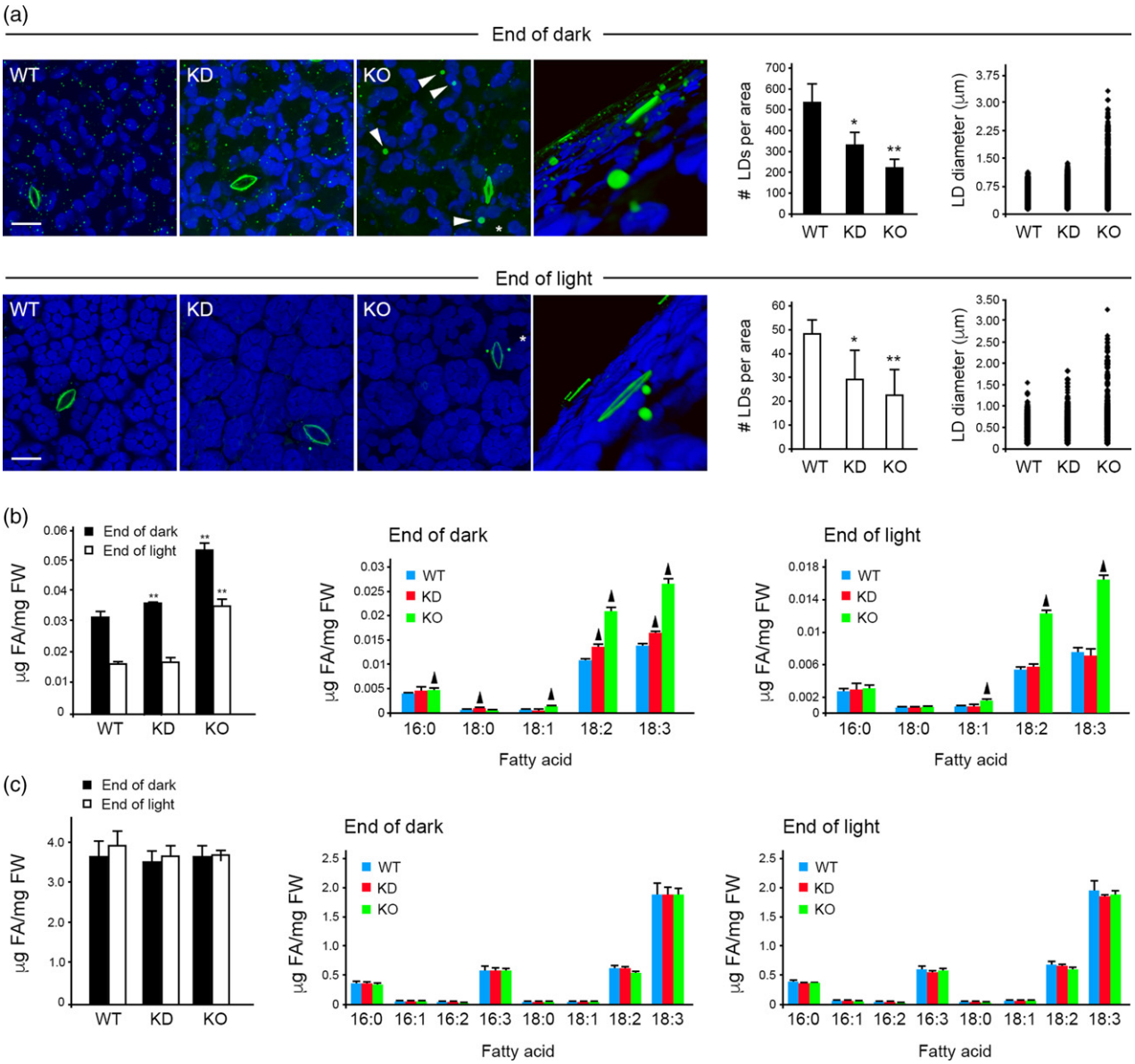

Figure 5. Effects of *LDIP* disruption on lipid droplets (LDs) and neutral lipid content in leaves.

(a) Abundance and size of LDs during the diurnal cycle in leaves of Arabidopsis *LDIP* mutant plants. Wild-type (WT) and *LDIP* knockout (KO) and knockdown (KD) mutant lines (Figure S7) were grown on ½ MS plates for 15 days in a 16-h/8-h day/night cycle, then leaves were harvested at the end of the night or end of the day, stained with BODIPY, and then the LDs examined by confocal laser-scanning microscopy. Representative images of BODIPY-stained LDs in leaves from each line (as indicated by labels) are shown on the left and quantifications of LD number per area and LD diameter are indicated by the graphs on the right. The blue colour in the micrographs is attributable to chlorophyll autofluorescence. Micrographs on the far right in each row of images are 3D projections of surface-rendered, high-magnification (zoom in) *Z*-stack images of a selected region of the same cells shown in micrographs of the KO leaves; asterisks represent the point of view for the 3D images and arrowheads indicate obvious examples of supersized LDs. Bars = 20 μm. Values of LD number are averages (±SD) from three biological replicates, each replicate consisting of eight leaf samples per line. LD diameter was calculated using the same data set (i.e. micrographs). Single and double asterisks in graphs represent statistically significant differences (relative to WT) at $P \leq 0.05$ and $P \leq 0.01$, respectively, as determined by Student's *t*-test.

(b) Neutral lipid content and composition of Arabidopsis leaves in 15-day-old seedlings at the end of the dark or end of the light period (as indicated in graph legends) in WT and *LDIP* KD or KO mutant lines. FA, fatty acids; FW, fresh weight. Asterisks and arrowheads represent statistically significant differences at $P \leq 0.01$ and $P \leq 0.05$, respectively, as determined by Student's *t*-test.

(c) Polar lipid content and composition of Arabidopsis leaves in 15-day-old seedlings at the end of the dark or end of the light in (as indicated in graph legends) WT and *LDIP* KD or KO mutant lines.

constituent of LDs in a recent proteomics study of LDs isolated from Arabidopsis senescing leaves (Brocard *et al.*, 2017).

We also showed that *LDIP* is present as a single-copy gene in Arabidopsis and, similar to the Arabidopsis *LDAP* genes (Gidda *et al.*, 2016; Kim *et al.*, 2016), is expressed in

a variety of organs and developmental stages, including seeds (Figure 2). Like the LDAPs (Horn *et al.*, 2013), as well as the oleosins (Huang and Huang, 2015), *LDIP* is strongly conserved amongst plant species (Figure 2), with no homologues detected outside the plant kingdom, indicating it is a plant-specific, LD-localized protein. Further, these general evolutionary similarities between LDIPs and LDAPs, taken together with their physical interaction (Figure 4), imply that they may have co-evolved in terms of a functional relationship.

LDIP is class II-type LD coat protein

LD proteins can target the LD surface either by binding the lipids of the phospholipid monolayer and/or neutral lipid core or by associating with other coat proteins (Kory *et al.*, 2016; Bersuker and Olzmann, 2017). In general, they are divided into two classes: class I proteins, including the oleosins, which target to the LD surface via the ER (Huang and Huang, 2017), and class II proteins, which target directly from the cytoplasm. When transiently overexpressed in tobacco leaf cells, Cherry-LDIP localized to LDs and the cytoplasm, but was never observed in association with the ER, even after extended periods of transient expression in tobacco (Figure S12) or when stably (ectopically) expressed in Arabidopsis plants (Figure S10), suggesting that LDIP is a class II-type LD protein.

Class II LD proteins typically possess one or more structural motifs that allow them to associate specifically with LDs, such as an amphipathic α-helix or hydrophobic domains (Kory *et al.*, 2016). Hydropathy analyses and 3D structural modelling revealed that amino acid residues 48–60 within Arabidopsis LDIP formed a potential amphipathic α-helix, followed by a downstream, strongly hydrophobic region (amino acids 107–211) (Figure 3) that had limited sequence similarity to the promethin proteins of mammals or MmpL proteins of mycobacteria. Subsequent mutational analyses showed that the N-terminal region of LDIP (i.e. $LDIP^{1–106}$), which contained the amphipathic α-helix, was both necessary and sufficient for LD targeting, while a mutant version of the protein (i.e. $LDIP^{107–249}$) containing the promethin/MmpL-like domain, but lacking the N-terminal region, targeted to the ER (Figure 3). This latter result might imply that the ER is important for some aspect(s) of LDIP targeting and/or function, as evidenced by LDIP being previously identified in the microsomal fraction of avocado mesocarp, while avocado LDAPs were enriched in purified LDs (Horn *et al.*, 2013). LDs are also known to maintain intimate associations with the ER (Chapman *et al.*, 2012; Gao and Goodman, 2015), and, as discussed in more detail below, perhaps LDIP is localized to ER–LD junctions prior to its localization to the LD surface. However, we also cannot rule out the possibility that the localization of the $LDIP^{107–249}$ mutant to the ER simply reflects an artefact of protein (mis)folding or a default targeting pathway, since hydrophobic proteins lacking their normal targeting information are often misdirected to the ER (Walter and Johnson, 1994).

LDIP–LDAP3 interactions and potential mechanisms of LDIP activity

LDIP was initially identified in a Y2H screen using LDAP3 as 'bait', and the physical association of LDIP and LDAP3 on LDs was confirmed using BiFC (Figure 4). Additional Y2H studies suggested that LDIP can form homotypic associations with itself (Figure 4) as well as bind to Arabidopsis LDAP1 and LDAP2, although relatively less so with LDAP1 (Figure S13). Nonetheless, all of these interactions were further supported by affinity-capture experiments, wherein GFP-tagged LDIP was transiently expressed in tobacco leaves then precipitated using affinity-capture methods, with co-purifying proteins, most notably the tobacco LDIP and LDAPs, being identified by MS and peptide mass fingerprinting (Figure 4).

In considering the functional significance of the LDIP–LDAP protein interaction, one hypothesis is that LDIP serves as an anchor for targeting LDAP to the LD surface. Prior studies have shown that recombinantly expressed and purified LDAP (LDAP3) binds weakly and non-specifically to synthetic liposomes containing various phospholipid compositions (Gidda *et al.*, 2016), indicating that other factors are probably involved in determining its LD-specific association. The LDAPs are also generally hydrophilic proteins, with no predicted membrane-spanning regions or other obvious regions of strong hydrophobicity (Gidda *et al.*, 2016). As such, they probably need to interact with other proteins for recruitment to and association with the LD surface, and given the strong hydrophobic domain within LDIP (Figure 4) it is possible that it serves as an anchor for this process. Alternatively, it is possible that the previously reported *in vitro* liposome-binding assays (Gidda *et al.*, 2016) did not faithfully recapitulate some needed, but as yet unknown, aspect of the targeting conditions, and thus LDAP might target specifically to LDs in a protein-independent manner *in vivo*, or through interaction with protein(s) other than LDIP.

Additional support for a functional connection between LDIP and LDAP comes from analyses of knockout mutants of both genes. We showed previously that disruption of any of the three *LDAP* genes in Arabidopsis decreased the number of LDs in 15-day-old leaves (Gidda *et al.*, 2016), and while we did not observe any apparent changes in the size of LDs, a recent study of a *LDAP1* knockout in Arabidopsis senescing (42–49 days old) leaves, which contain more neutral lipid than younger leaves, did show both a decrease in the number of LDs and an increase in

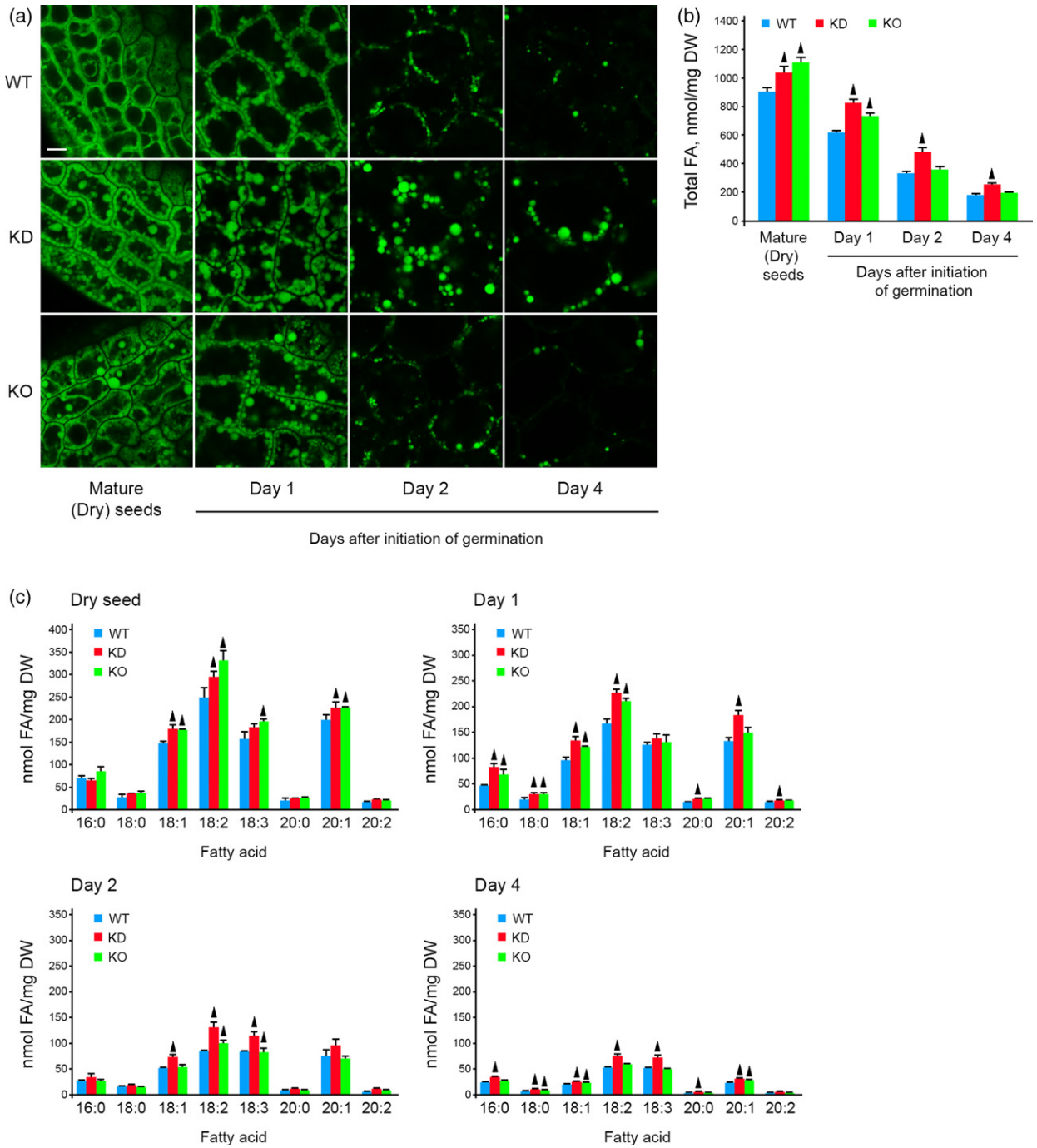

Figure 6. Effects of *LDIP* disruption on seed development and post-germinative growth.
(a) Representative confocal laser-scanning microscopy images of BODIPY-stained lipid droplets (LDs) in mature, dry seeds and seedlings 1, 2 or 4 days after the onset of germination of wild type (WT) and *LDIP* knockdown (KD) or knockout (KO) mutant lines. Note the presence of larger LDs in the KD and KO seeds and seedlings. Bar = 5 μm.
(b) Total lipid content on a fatty acid basis in WT and *LDIP* KD and KO mutant mature seeds and in seedlings during post-germinative growth. DW, dry weight; FA, fatty acids. Results shown (and in (c)) represent averages (±SD) of three biological replicates, and arrowheads represent statistically significant differences at $P \leq 0.05$ determined by Student's *t*-test.
(c) Fatty acid composition in WT and *LDIP* KD and KO mutant mature seeds and in seedlings during post-germinative growth.

variability of LD size, with the appearance of some noticeably larger LDs (Brocard *et al.*, 2017). This phenotype is generally similar to the *LDIP* mutant phenotype described here, which included a reduction in the number of LDs in leaves and an increase in the variability of LD size, with the appearance of some considerably larger LDs (i.e.

supersized LDs) (Figure 5). One potential model for explaining these observations is that, as mentioned above, LDIP is required for the association of LDAP with LDs, which are subsequently important for stabilizing the LDs and preventing LD–LD fusion, as previously proposed (Gidda *et al.*, 2016). In the absence of LDIP, LDAPs would not associate with LDs as effectively, leading to a reduction of LDAP proteins on the LD surface and a concomitant increase in the propensity for LDs to fuse in the cytoplasm. In this model, fusion of LDs would not only reduce LD abundance but also lead to increases in the size of LDs. The increase in LD size might also account for the observed increase in neutral lipid content in *LDIP* mutant plants, since the lower surface-to-volume ratio of larger LDs would potentially reduce access of their TAG contents to lipase enzymes. There is, however, an important difference in the phenotypes of *LDIP* and *LDAP* mutant plants: disruption of *LDAP*s resulted in no change in the total neutral lipid content of leaves (Gidda *et al.*, 2016; Kim *et al.*, 2016), while disruption of *LDIP* nearly doubled the amount of leaf oil (Figure 5). This suggests that (i) LDIP has functions beyond just the recruitment and association of LDAP to LDs and/or (ii) the model for interaction of LDIP and LDAP is more complex, and the similarities in the LD phenotypes of the *LDIP* and *LDAP* mutants arise from distinct underlying molecular mechanisms.

Disruption of *LDIP* in seeds also resulted in the appearance of supersized LDs in the seed embryo and significant increases in total seed oil content (Figure 6). At the cell biology level, this enlarged LD phenotype is reminiscent of the phenotype observed in *oleosin* KO mutants, where a reduction of oleosin results in fusion of LDs in developing seeds (Siloto *et al.*, 2006; Schmidt and Herman, 2008; Shimada *et al.*, 2008; Miquel *et al.*, 2014). At the biochemical level, however, seed oil content is reduced in the *oleosin* mutant background (Siloto *et al.*, 2006) while it is increased in the *LDIP* mutants. Indeed, in two different organ types (leaves and seeds) and two different developmental stages (mature seeds and 15-day-old leaves), disruption of *LDIP* not only affects LD size but also increases total neutral lipid content (Figures 5 and 6). On the other hand, this cellular and biochemical phenotype is more similar to the phenotype observed when the Arabidopsis *SEIPIN1* gene is overexpressed in transgenic plants (Cai *et al.*, 2015). SEIPIN proteins are conserved ER membrane proteins that localize specifically to ER–LD junctions and promote LD formation (Chen and Goodman, 2017). The SEIPINs are also known to form large multimeric complexes that recruit and interact with multiple protein partners, thereby serving as important organizing centres for LD production. Although SEIPIN has no known enzymatic functions, SEIPINs in yeast and mammals interact with several different enzymes of the Kennedy pathway (Sim *et al.*, 2013; Talukder *et al.*, 2015; Pagac *et al.*, 2016), which couples LD formation with localized synthesis of neutral lipids, including metabolites such as diacylglyercol and phosphatidic acid that are known to be essential for LD formation (Pol *et al.*, 2014). Also key to the growth of nascent LDs is the coordinated synthesis and enrichment of certain phospholipids within the LD monolayer. As such, the composition of the phospholipid monolayer is an important determinant of the size of LDs, as well as their propensity for subsequent LD–LD fusion (Thiam *et al.*, 2013; M'barek *et al.*, 2017). Indeed, the majority of genes identified in screens for altered LD sizes in insect and yeast cells are involved in phospholipid metabolism (Guo *et al.*, 2008; Fei *et al.*, 2011; Li *et al.*, 2016; Fan *et al.*, 2017).

Given that the size of LDs is affected in *LDIP* mutants and there is an increase in neutral lipid content (Figures 5 and 6), and that SEIPIN is one of the LD proteins that co-purified with LDIP in affinity-capture experiments in tobacco (Figure 4), one possibility is that LDIP functions at an earlier step in LD biogenesis that also involves SEIPIN activity. For instance, LDIP might serve at the cytoplasmic surface of ER–LD junctions to modulate the phospholipid content of a growing nascent LD, thereby affecting local glycerolipid metabolism, which is also influenced by SEIPIN activity. In the absence of LDIP, however, phospholipids might be altered or reduced, thereby promulgating larger LDs and/or the fusion of normal-sized LDs into supersized LDs, and redirecting glycerolipid intermediates from phospholipid metabolism to neutral lipid synthesis. In this scenario, LDIP would function as part of the machinery that helps coordinate the ordered formation of nascent LDs of a specific size and composition. Moreover, LDIP could still serve as an anchor for the recruitment of LDAPs to the growing LDs, although in seeds the LDAPs may be supplanted by the oleosin proteins.

Lastly, it is also possible that LDIP might serve at a later step in the LD life cycle by transferring neutral lipids from LDs to other organelles. The hydrophobic MmpL domains within mycobacterial MmpL proteins are known to associate to form complexes that transport various lipid compounds across the plasma membrane to the outer cell wall (Viljoen *et al.*, 2017). Based on its MmpL-like domain sequence (Figure 3) and its ability to self-associate (Figure 4), perhaps LDIP, in an analogous manner, is involved in the transfer of lipids from LDs in plant cells, such that disruption of *LDIP* results in the continued growth of LDs and a subsequent increase in cellular neutral lipid content. This model is somewhat difficult to reconcile in seeds, however, where oil production is known to include both rapid synthesis of oil as well as some turnover in the latter stages of seed development due to peroxisomal β-oxidation (Theodoulou and Eastmond, 2012). While a reduced transfer of lipids from LDs to peroxisomes in *LDIP* mutant seeds might account for the increase in seed oil content of mature seeds, there is apparently no defect in the

mobilization of seed oil during post-germination growth, i.e. the elevated seed oil content in mature *LDIP* mutants seeds was rapidly degraded and achieves nearly wild-type levels in 4-day-old seedlings (Figure 6). Furthermore, disruption of *LDIP* results in a decrease in LD abundance in leaves (Figure 5), which would not be expected if LDIP served primarily in the transfer of neutral lipids out of LDs. As such, if LDIP is indeed involved in lipid transfer, it is perhaps more likely that the activity is required for modulating the phospholipid content of the monolayer, either during LD formation, as discussed above, or during a later stage in the lifecycle of mature LDs. Current studies are now aimed at distinguishing between these various possibilities and also determining whether LDIP is required for the targeting of LDAPs to LDs.

EXPERIMENTAL PROCEDURES

Plant material, growth conditions and transformations

All Arabidopsis (*Arabidopsis thaliana*)-based experiments employed the WT Columbia-0 (Col-0) ecotype and derivatives thereof, including the T-DNA insertional mutant lines [i.e. *LDIP*-KD (SALK_084555) and *LDIP*-KO (SAIL_335_H11)] obtained from the Arabidopsis Biological Resource Center (ABRC; https://abrc.osu.edu). Unless indicated otherwise, Arabidopsis plants were cultivated in soil in an environmental room with a 16-h/8-h day/night cycle at 22°C and 50 μE m^{-2} sec^{-1} light intensity, or seeds were sterilized and plated on plates containing ½ MS media (Murashige and Skoog, 1962), then stratified for 3 days in the dark at 4°C before being moved into a growth chamber for the initiation of germination, with similar growth conditions to those described above. For the WT × *ldip* KO cross, F_1 and F_2 seeds (progeny) were collected and plated on full-strength MS plates containing 50 μg μl^{-1} Basta (phosphinothricin; Gold Biotechnology, https://www.goldbio.com/). BODIPY-stained LDs in all F_1 and F_2 seedlings that survived selection were analysed by CLSM and a chi-square test was used to determine the significance of the segregation pattern of the F_2 progeny. *LDIP*-KO plants were stably transformed (via *A. tumefaciens* infiltration, strain GV3101) with pMDC32/mCherry-LDIP using the floral dip method (Clough and Bent, 1998). The procedures for *A. tumefaciens* growth, transformation, infiltration and processing of leaf material for microscopy have been described elsewhere (McCartney *et al.*, 2005; Cai *et al.*, 2015).

Nicotiana benthamiana plants used for all *A. tumefaciens*-mediated transient expression experiments were grown in soil at 22°C with a 16-h/8-h day/night cycle and 50 μE m^{-2} sec^{-1} light intensity. Leaves of 28-day-old *N. benthamiana* plants were infiltrated with *A. tumefaciens* (strain LBA4404 or, for co-immunopreciptations, GV3101) carrying selected binary vectors. *Agrobacterium tumefaciens* transformed with the tomato bushy stunt virus gene *P19* was also included in all infiltrations to enhance transgene expression (Petrie *et al.*, 2010).

Gene cloning and plasmid construction

Molecular biology reagents were purchased from New England Biolabs (https://www.neb.com/), Thermo Fisher Scientific (https://www.thermofisher.com/) or Invitrogen (http://www.invitrogen.com/), and custom oligonucleotides were synthesized by Sigma-Aldrich (http://www.sigmaaldrich.com/). Sequence information for all primers used in gene cloning and plasmid construction is available upon request. All DNA constructs were verified using automated sequencing performed at the University of Guelph Genomics Facility. Plasmids harbouring full-length open reading frames (ORFs) for each of the candidate proteins identified in the LDAP3 Y2H screen, including LDIP, were obtained from the ABRC, then ORFs were PCR-amplified and subcloned into the plant expression binary vector pMDC43 using Gateway technology (Curtis and Grossniklaus, 2003). pMDC43 contains the ORF of dimeric GFP, followed by a multiple cloning site (MCS), and the 35S cauliflower mosaic virus promoter [as do all other plant expression vectors used in this study, with the exception of LDIPp::Cherry-MMPL (see below)]. pMDC43/mGFP-LDIP, consisting of a monomerized version of GFP (mGFP) linked to the N terminus of LDIP, was generated using PCR-based site-directed mutagenesis, whereby the leucine at position 221 in the GFP ORF in pMDC43/GFP-LDIP (serving as the template DNA) was replaced with a lysine (Zacharias *et al.*, 2002). pMDC32/Cherry-LDIP was constructed by amplifying the full-length ORF of *LDIP* and cloning the resulting PCR products into pRTL2/Cherry, a plant expression vector containing the monomeric red fluorescent protein Cherry (Gidda *et al.*, 2011). Thereafter, the coding region for the Cherry-LDIP fusion protein was subcloned into pMDC32 using Gateway technology. All the truncation and site-specific mutations of Cherry-LDIP used for analysing the putative LD targeting of LDIP signal were generated by PCR-based site-directed mutagenesis with pRTL2/Cherry-LDIP or pRTL2/Cherry-$LDIP^{1–106}$ as a template, followed by subcloning into pMDC32. pMDC32/GFP and pMDC32/Cherry, respectively encoding GFP and Cherry alone, and serving as cytoplasmic marker proteins, were constructed by amplifying the ORF of each fluorescent protein from pRTL2/GFP (Clark *et al.*, 2009) or pRTL2/Cherry, then subcloning into pMDC32. pMDC99/LDIPp::Cherry-MMPL, consisting of Cherry-LDIP driven by the native *LDIP* promoter sequence, was constructed by PCR amplifying (with genomic DNA as template) the 490-nucleotide sequence upstream of the *LDIP* ORF (and downstream of the ORF adjacent to *LDIP* in the Arabidopsis genome) then subcloning the resulting PCR products into pRLT2/Cherry-MMPL. Thereafter, the entire LDIPp::Cherry-MMPL sequence was cloned into pMDC99 using Gateway technology.

Plasmids used for BiFC assays were generated based on the Gateway-compatible vectors pDEST-VYNE/nVenus and pDEST-SCYCE/cCFP, which encode the N-terminal and C-terminal halves of Venus and CFP, respectively (Gehl *et al.*, 2009), and were obtained from the ABRC. The full-length ORF of LDIP and LDAP3 or LDAP3ΔC100, whereby a premature stop codon was introduced into the LDAP3 ORF, resulting in a 100-amino-acid long C-terminal truncation (Gidda *et al.*, 2016), were PCR-amplified from their respective pRTL2-based plasmids and then subcloned into pDEST-VYNE/nVenus or pDEST-SCYCE/cCFP using Gateway technology.

Other plant expression binary vectors used in this study have been described elsewhere, including the following: pMDC32/LDAP3-Cherry and OLEO1-mGFP, encoding Arabidopsis LDAP3 and oleosin isoform 1 appended to Cherry and mGFP, respectively (Horn *et al.*, 2013; Gidda *et al.*, 2016); ST-mRFP, encoding the N terminus of a rat *trans*-Golgi sialyl transferase appended to the monomeric red fluorescent protein (Boevink *et al.*, 1998); pBIN/ER-GK and pBIN/ER-RK, encoding ER (lumen)-localized green and red fluorescent fusion proteins, and referred to in this study as GFP-ER and RFP-ER, respectively (Nelson *et al.*, 2007) [obtained from the ABRC, clone numbers CD3-955 and CD3-959); pMDC32/Cherry-PTS1, encoding Cherry linked to type 1 peroxisomal matrix targeting signal and referred to in this study as Cherry-Perox (Ching *et al.*, 2012); and pORE04/LEC2 and pORE04/P19, encoding

Arabidopsis LEC2, a regulator of seed development, and the tomato bushy stunt virus RNA-silencing suppressor p19 (Petrie *et al.*, 2010).

For Y2H library screening, the full-length ORF of Arabidopsis LDAP3 was PCR-amplified from pRTL2/LDAP3-Cherry (Gidda *et al.*, 2016) then subcloned into the 'bait' vector pGBKT7-DNA-BD (Clontech). Similarly, for directed Y2H assays, the LDAP3 ORF was subcloned from pRTL2/LDAP3-Cherry into the 'prey' vector pGADT7-AD, and the ORF of Arabidopsis LDIP was PCR-amplified from a plasmid encoding the full-length LDIP ORF obtained from the ABRC (see above) and cloned into pGADT7-AD and pGBKT7-DNA-BD. pGADT7-AD/LDAP3ΔC100 was generated using PCR-based site-directed mutagenesis with pGADT7-AD/LDAP3 serving as the template.

LD isolations and intensity-based quantification (iBAQ) label-free proteomics

Two hundred and fifty milligrams of Arabidopsis seed (Col-0) was sterilized and stratified for 4 days in the dark at 4°C and then grown for 2 days in long-day conditions at 22°C on ½ MS medium plates without sucrose. Seedlings were ground in sand and 4 ml of grinding buffer [10 mM sodium phosphate buffer, pH 7.4, 0.5 mM Lohman's reagent and 10 mM *N*-ethylmaleimide (Sigma-Aldrich)] for 1 min with a mortar and pestle. The resulting homogenate was spun for 10 sec at 100 ***g*** and a 100 μl aliquot of the supernatant ('total cell protein' sample) was precipitated in 90% (v/v) ethanol at −20°C. The rest of the supernatant was centrifuged at 20 000 ***g*** for 20 min at 4°C and the resulting fat pad was washed twice with grinding buffer and finally delipidated in ethanol at −20°C. The protein pellet ('LD fraction' sample) was washed twice with ethanol, dried and resuspended in 6 M SDS and 5% (w/v) urea. Protein concentrations were determined with a Pierce BCA protein assay kit (Thermo Fisher Scientific). Ten micrograms of protein was run on a 12% SDS-PAGE gel until it entered into the separation gel. The Coomassie blue-stained protein bands were then excised and processed as described by Shevchenko *et al.* (1996). Peptides were desalted over a Supelco C18 column (Sigma-Aldrich) according to Rappsilber *et al.* (2007) and then subjected to LC-MS/MS (Schmidtt *et al.*, 2017). Protein abundance was quantified using iBAQ label-free quantification implemented in MaxQuant software (Schaab *et al.*, 2012) and the values were calculated as a percentage of all values in one sample. For a detailed description of the data acquisition and processing see Methods S1. The MS proteomics data have been deposited to the ProteomeXchange Consortium via the PRIDE partner repository (Vizcaíno *et al.*, 2016) with the dataset identifier PXD007192.

For Western blotting, protein extracts were separated by SDS-PAGE and electroblotted onto Hybond® nitrocellulose (GE LifeSciences, Mississauga, ON, Canada). Membranes were then incubated with anti-LDIP IgGs and immunoreactive proteins visualized using a Western Lightning® Plus-ECL kit and Blue XB film (PerkinElmer, Waltham, MA, USA). Rabbit anti-LDIP IgGs raised against a synthetic peptide corresponding to the LDIP amino acid sequence, -CNTISRHQHQDREVNIESTN- (residues 231–249), and purified using an LDIP peptide-Sepharose-linked column were generated by Cedarlane Labs (https://www.cedarlanelabs.com/).

Bioinformatics

Construction of the LDIP phylogenetic tree was carried out using BioEdit (v.7.2.5) (Hall, 1999) with sequence alignments performed using the embedded ClustalW software, followed by manual adjustment, and phylogenetic reconstruction of the aligned sequences performed using the embedded ProML Protein Maximum Likelihood program. The phylogram was generated using TreeView (v.1.6.6) (Page, 1996). Polypeptide sequences of various LDIP proteins were identified using the Protein Homologs tool at Phytozome (http://www.phtozome.net) (Goodstein *et al.*, 2011). Other protein sequence alignments were performed using the ClustalW algorithm at Prabi-Gerland (https://npsa-prabi.ibcp.fr/). Hydropathy analyses of amino acid sequences were carried out using the TMHMM server (http://www.cbs.dtu.dk/services/TMHMM/) and helical wheel projections were generated using HeliQuest (http://heliquest.ipmc.cnrs.fr) (Gautier *et al.*, 2008). Structural homology modelling was conducted using SWISS-MODEL (https://swissmodel.expasy.org) (Biasini *et al.*, 2014), whereby the Arabidopsis LDIP polypeptide sequence was used as a query to search for templates, then a structural homology model was built for the N-terminal region of LDIP (amino acid residues 32–115) using default parameters.

RT-PCR and genotyping

Assessment of *LDIP* gene expression in leaves of 15-day-old WT Arabidopsis and T-DNA transgenic lines, as well as the expression of *LDIP* and *LDAP3* BiFC constructs in infiltrated *N. benthamiana* leaves, was carried out using RT-PCR based on procedures described by Cai *et al.* (2015) and Gidda *et al.* (2016). *LDIP* and *LDAP3* were amplified by 30 cycles of 94°C for 30 sec, 55°C for 30 sec and 72°C for 90 sec, while *TUBULIN*, *ACTIN* and *EF1α*, serving as control genes, were amplified by 30 cycles of 94°C for 30 sec, 55°C for 30 sec and 72°C for 1 min. All reactions contained 500 ng of total RNA. Specific forward and reverse primers used for RT-PCRs, as well as those used for genotyping of *LDIP* T-DNA insertional transgenic lines, are provided in Table S3.

Microscopy

Wild-type and transgenic Arabidopsis seeds and leaves, as well as *A. tumefaciens*-infiltrated tobacco leaves, were processed for CLSM imaging, including staining of LDs either with BODIPY 493/503 (Invitrogen), Nile red (Sigma-Aldrich) or MDH (Abgent, http://www.abgent.com/), as previously described (Cai *et al.*, 2015; Gidda *et al.*, 2016). Micrographs of Arabidopsis and tobacco leaves were acquired using either a Leica DM RBE microscope equipped with a 63× Plan Apochromat oil-immersion objective and TCS SP2 scanning head, or a Leica SP5 CLSM equipped with a Radius 405-nm laser (Leica Microsystems, https://www.leica-microsystems.com/). Micrographs of dry seeds and germinated seedlings were acquired with a Zeiss LSM710 with a 63× water-immersion objective lens (Carl Zeiss Inc., https://www.zeiss.com/). Excitations and emission signals for fluorescent proteins, LD stains and/or chlorophyll autofluorescence collected sequentially as single optical sections or *Z*-series in double- or triple-labelling experiments are the same as those described in Gidda *et al.* (2016); single-labelling experiments showed no detectable cross-over at the settings used for data collection. 3D volume renderings were generated using Volocity imaging software (v.6.3) (PerkinElmer, http://www.perkinelmer.com/). The numbers and diameters of LDs in leaves of Arabidopsis seedlings were quantified according to Cai *et al.* (2015) using the Analyze Particles function in ImageJ (v.1.43; https://imagj.net), and the significance assessments of these data sets were performed using Student's *t*-test. All fluorescence images of cells shown in individual figures are representative of at least two separate experiments, including at least three separate transformations of tobacco leaf cells. Figure compositions

were generated using Adobe Photoshop CS (Adobe Systems, http://www.adobe.com/).

Y2H and BiFC assays

Screening of a Y2H library, consisting of Arabidopsis cDNA from various plant tissues and cloned into the appropriate prey vector, using Arabidopsis LDAP3 (pGBKT7/LDAP3) as 'bait', was carried out with the Matchmaker Gold Y2H System (Clontech Laboratories, Inc., http://www.clontech.com/) as described by the manufacturer. All yeast strains that grew on low-selection [synthetic dextrose (SD) media lacking tryptophan and leucine, but containing X-α-Gal and Aureobasidin A] or high-selection (the same as low-selection media, but also lacking histidine and adenine) were designated as 'weak' or 'strong' interactors, respectively. Plasmids were extracted from yeast cells to determine the identity of encoded prey proteins using DNA sequencing. None of the prey plasmids autoactivated the Y2H reporter genes when retransformed into yeast cells with appropriate corresponding empty vectors. Directed Y2H assays were carried out as described previously (Richardson *et al.*, 2011), and, unlike for Y2H screening, plates used for high-stringency growth conditions consisted of SD media lacking tryptophan, leucine, histidine and adenine. The results of growth assays shown in figures are representative of those obtained from analysing three isolated yeast colonies from at least two independent transformations. In addition, all fusion proteins were confirmed to be expressed properly by Western blot analysis, as described above.

The BiFC assays in tobacco leaves were performed according to Stefano *et al.* (2015). Briefly, leaves were infiltrated with *Agrobacterium* containing plasmids encoding cCFP-LDIP and nVenus appended to either LDAP3 or LDAP3ΔC100, the latter serving as a negative control based on guidelines described elsewhere for assessing protein interactions using the BiFC assay (Lee *et al.*, 2012). All infiltrations also included Cherry-Perox, serving as a transformation marker. Transformed cells in leaf areas were visualized (via CLSM) based on Cherry fluorescence, and both Cherry and reconstituted BiFC (cCFP/nVenus) fluorescence signals were collected with identical image acquisition settings for all samples analysed. ImageJ was used to quantify spectral counts from acquired micrographs of at least 20 leaf areas from three separate infiltrations. CLSM acquisition settings, amounts of *Agrobacterium* infiltrated and post-infiltration times were chosen based on preliminary optimization experiments aimed at minimizing the possibility of non-specific interactions based on guidelines for assessing protein–protein interactions using the BiFC assay described by Stefano *et al.* (2015).

Analysis of lipids

For analysis of the content and fatty acid composition of neutral and polar lipids from Arabidopsis leaves, total lipids were extracted from 500 mg (fresh weight, FW) of 15-day-old seedlings grown on ½ MS medium, using a hexane/isopropanol method (Hara and Radin, 1978) with the addition of C17:0 TAG (Sigma-Aldrich) and C15:0 phosphatidychloline (Avanti Polar Lipids, Inc., https://avantilipids.com/) as internal standards. Total lipid extracts in hexane were separated into neutral and polar lipids on solid-phase extraction cartridges (Supelco Discovery DSC-Si 6 ml, Sigma-Aldrich), as described (Gidda *et al.*, 2016). To prepare fatty acid methyl esters (FAMEs), 0.5 ml of 0.5 N sodium methoxide solution in methanol was added to neutral or polar lipid extracts, and samples were incubated at room temperature (22°C) for 25 min. The reaction was quenched with 1 ml of saturated NaCl solution in water, and FAMEs were extracted with 1 ml of hexane. The FAME samples were analysed on an Agilent HP 6890 series GC system equipped with a 7683 series injector and autosampler (Agilent Technologies, http://www.agilent.com/) and a BPX70 (SGE Analytical Science, http://www.sge.com/) capillary column (10 m × 0.1 mm × 0.2 mm) with a constant pressure of 25 p.s.i., as described in Gidda *et al.* (2016). Compounds were identified by comparing with the GLC-10 FAME standard mix (Sigma-Aldrich). Analyses of the content and fatty acid composition of neutral and polar lipids from dry seeds and germinated seeds were performed as described in Gidda *et al.* (2016).

Co-immunoprecipitation using GFP-Trap-A beads

Leaves of approximately 28-day-old *N. benthamiana* plants were transiently transformed (via *Agrobacterium* infiltration) with binary plasmids encoding GFP alone or GFP-LDIP and with and without LEC2. Expression of GFP and GFP-LDIP was verified by CLSM and transformed leaves were collected (3 days post-infiltration) for protein extraction. Briefly, approximately 1.5 g of leaf material was ground to a fine powder in liquid nitrogen using a mortar and pestle. Then 3 ml of extraction buffer [50 mM TRIS-HCl, pH 7.5, 150 mM NaCl, 10% glycerol, 1% NP-40, 1 mM PMSF, Roche protease inhibitor cocktail (2 tablets/10 ml buffer)] (Roche Diagnostics, http://www.roche.com/) was added to the tissue powder; samples were transferred into 15-ml test tubes and incubated for 30 min on ice and vortexed every 10 min. Cell lysates were centrifuged at 2500 ***g*** at 4°C for 10 min to remove cell debris and the supernatants were further clarified by centrifugation at 16 000 ***g*** at 4°C for 20 min. Supernatants were then incubated with 30 μl of GFP-Trap-A beads (ChromoTek, https://www.chromotek.com/) for 3 h at 4°C on a rotating shaker. After incubation, beads were washed four times with extraction buffer and proteins bound to the beads were then eluted with 100 μl of 4× SDS sample buffer and heated at 70°C for 10 min. To confirm the presence of the 'bait' proteins (i.e. free GFP or GFP-LDIP), an aliquot of each immunoprecipitated sample was separated by SDS-PAGE and detected by Western blotting with anti-GFP antibodies (Thermo Fisher Scientific). The remaining protein was concentrated at the top of an SDS-PAGE resolving gel and the Coomassie blue-stained protein bands were excised and submitted to the Michigan State University Proteomics Core Service (https://rtsf.natsci.msu.edu/proteomics/).

Processing of samples (gel bands) for MS analysis was carried out by dehydrating the samples using 100% acetonitrile and incubating with 10 mM dithiothreitol in 100 mM ammonium bicarbonate (pH ~8) at 56°C for 45 min, followed by dehydration and incubation in the dark with 50 mM iodoacetamide in 10 mM ammonium bicarbonate for 20 min. Gel bands were then washed with ammonium bicarbonate and dehydrated again. Sequencing-grade modified trypsin (0.01 μg μl^{-1}) in 50 mM ammonium bicarbonate was added to the gel band and incubated at 37°C overnight. Peptides were extracted by water bath sonication in a solution of 60% acetonitrile and 1% trichloroacetic acid, vacuum dried to about 2 μl and then re-suspended in 2% acetonitrile/0.1% trifluoroacetic acid to 25 μl. Five microlitres was automatically injected by a Thermo EASYnLC 1000 (Thermo Fisher Scientific) onto a Thermo Acclaim PepMap 0.1 mm × 20 mm C18 peptide trap and washed for about 5 min. Bound peptides were then eluted onto a Thermo Acclaim PepMap RSLC 0.075 mm × 250 mm C18 column over 65 min with a gradient of 5% to 28% buffer B (consisting of 99.9% acetonitrile and 0.1% formic acid) in 54 min, ramping to 100% buffer B at 55 min and held at 100% buffer B for the duration of the run at a constant flow rate of 0.3 μl min^{-1}. Eluted peptides were sprayed into a Thermo Fisher

Q-Exactive MS using a FlexSpray spray ion source. Survey scans were taken in the Orbitrap (70 000 resolution, determined at *m*/*z* 200) and the top 10 ions in each survey scan were then subjected to automatic higher-energy collision-induced dissociation with fragment spectra acquired at 17 500 resolution. The resulting MS/MS spectra were converted to peak lists using Mascot Distiller (v.2.6.1; http://www.matrixscience.com/) and searched against a database of all *N. benthamiana* protein sequences available from the Sol Genomics Network (v.0.4.4; http://www.solgenomics.net) and appended with common laboratory contaminants (cRAP project; http://www.thegpm.orgt) using the Mascot searching algorithm (v.2.6.0). The Mascot output was then analysed using Scaffold (v.4.7.5; http://www.proteomesoftware.com/) to probabilistically validate protein identifications. Assignments validated using the Scaffold 1% false discovery rate (FDR) confidence filter are considered true. Mascot parameters for all databases were as follows: (i) allow up to two missed tryptic sites; (ii) fixed modification of carbamidomethyl cysteine, variable modification of oxidation of methionine, deamidation of glutamine and asparagine; (iii) peptide tolerance of ±10 p.p.m.; (iv) MS/MS tolerance of 0.3 Da; and (v) FDR calculated using randomized database search.

ACCESSION NUMBERS

Arabidopsis Information Resource numbers and/or GenBank accession numbers for the Arabidopsis proteins described in this study are as follows: LDIP (At5g16550, NP_568333), LDAP3 (At3g05500, NP_187201), EIF2 (At2g39990, NP_181528), MSR1 (At3g21190, NP_566677), TPR8 (At4g08320, NP_001031594), PRA7 (At1g55190, NP_564679), NUDT3 (At1g79690, NP_565218), TRA2 (At5g13420, NP_196846), ATMS1 (At5g17920, NP_001078599), and PGL5 (At5g24420, NP_197830), OLEO1 (At4g25140, NP_194244), α-TUBULIN (At5g44340, NM_123801), and LEC2 (At1g28300, NP_564304). Other protein accession numbers: tomato bushy stunt virus p19 (CAC01278) and *N. benthamiana* ACTIN (AY179605). Accession numbers for LDIP homologues from various plant species used in the construction of the phylogenetic tree (Figure 2) and the protein sequence alignment (Figure 3) are provided in Table S4.

ACKNOWLEDGEMENTS

We are grateful to Dr Reynald Tremblay (University of Guelph) for assistance with the phylogenetic analysis of LDIPs, Dr Frederica Brandizzi (Michigan State University) for ST-mRFP, Dr Qing Liu (CSIRO Plant Industry) for pORE04/LEC2 and pREO4/P19 and Ms Vivien Truong (University of Guelph) for assistance with figure construction. We are also grateful to Drs Toby Kellogg and Michael McKain (Donald Danforth Plant Science Center) for their insights on the potential co-evolution of LDIPs and LDAPs, and Drs Jay Thelen and Veronika Lancikova (University of Missouri-Columbia) for their assistance with preliminary LD proteomics experiments. Proteomics analysis of GFP capture experiments was carried out by Douglas Whitten (Michigan State University Proteomics Core Facility). Research support was provided by the US Department of Energy (DOE) Office of Science, BES-Physical Biosciences program (DE-SC0016536), the Natural Sciences and Engineering Research Council of Canada (217291-2013), the German Research Foundation (DFG) and the Studienstiftung des Deutschen Volkes. Mention of trade names or commercial products in this article is solely for the purpose of providing specific information and does not imply recommendation or endorsement by the US Department of Agriculture (USDA). The USDA is an equal opportunity provider and employer.

CONFLICT OF INTEREST

All the authors declare that they have no conflict of interests.

SUPPORTING INFORMATION

Additional Supporting Information may be found in the online version of this article.

Figure S1. Localization of GFP-tagged candidate LDAP3-interacting proteins in tobacco leaf epidermal cells.

Figure S2. Localization of Cherry-tagged LDIP truncation mutants and modified variants thereof in tobacco leaf epidermal cells.

Figure S3. Helical wheel projections of N-terminal polypeptide sequences from selected LDIP homologues.

Figure S4. Yeast two-hybrid growth assays with Arabidopsis LDIP and LDAP3.

Figure S5. Western blot analysis of yeast two-hybrid fusion proteins.

Figure S6. Confirmation of expression of bimolecular fluorescence complementation fusion constructs in tobacco leaf epidermal cells using RT-PCR.

Figure S7. Characterization of Arabidopsis *LDIP* T-DNA insertional transgenic lines.

Figure S8. BODIPY-stained lipid droplets in leaves of 28-day-old Arabidopsis wild-type and *LDIP* knockout plants.

Figure S9. Progeny analysis and BODIPY-stained lipid droplets in leaves of Arabidopsis F_1 and F_2 plants from a wild type × *LDIP* knockout mutant backcross.

Figure S10. BODIPY-stained lipid droplets in leaves of Arabidopsis wild type and various *LDIP* knockout mutant and transgenic plants, and the localization of Cherry-LDIP in a stably transformed *LDIP* knockout Arabidopsis plant.

Figure S11. RT-PCR analysis of modified *LDIP* transcripts in the *LDIP* knockout mutant.

Figure S12. Localization of over-expressed Cherry-LDIP in tobacco leaf epidermal cells.

Figure S13. Interaction of Arabidopsis LDIP and LDAP1 and LDAP2 in yeast cells.

Table S1. Quantitative proteomics data from 2-day-old Arabidopsis seedling total cell extracts and isolated lipid droplets.

Table S2. Qualitative proteomics data depicting identified peptides.

Table S3. List of primers used for RT-PCR and genotyping.

Table S4. Accession numbers of LDIP homologues from various plant species.

Methods S1. Detailed workflow of proteomics data acquisition and processing.

REFERENCES

Barneda, D. and Christian, M. (2017) Lipid droplet growth: regulation of a dynamic organelle. *Curr. Opin. Cell Biol.* **47**, 9–15.

Bersuker, K. and Olzmann, J.A. (2017) Establishing the lipid droplet proteome: mechanisms of lipid droplet protein targeting and degradation. *Biochim. Biophys. Acta* **1862**, 1166–1177. https://doi.org/10.1016/j.bbalip.2017.06.00

Berthelot, K., Peruch, F. and Lecomte, S. (2016) Highlights on *Hevea brasiliensis* (pro) hevein proteins. *Biochimie*, **127**, 258–270.

Biasini, M., Bienert, S., Waterhouse, A. *et al.* (2014) SWISS-MODEL: modelling protein tertiary and quaternary structure using evolutionary information. *Nucleic Acids Res.* **42**(W1), W252–W258.

Boevink, P., Oparka, K., Cruz, S.S., Martin, B., Betteridge, A. and Hawes, C. (1998) Stacks on tracks: the plant Golgi apparatus traffics on an actin/ER network. *Plant J.*, **15**, 441–447.

Brocard, L., Immel, F., Coulon, D., Esnay, N., Tuphile, K., Pascal, S., Claverol, S., Bessoule, J.J. and Bréhélin, C. (2017) Proteomic analysis of lipid droplets from Arabidopsis aging leaves brings new insight into their biogenesis and functions. *Front. Plant Sci.* **8**, 894.

Cai, Y., Goodman, J.M., Pyc, M., Mullen, R.T., Dyer, J.M. and Chapman, K.D. (2015) Arabidopsis SEIPIN proteins modulate triacylglycerol accumulation and influence lipid droplet proliferation. *Plant Cell*, **27**, 2616–2636.

Chapman, K.D., Dyer, J.M. and Mullen, R.T. (2012) Biogenesis and functions of lipid droplets in plants Thematic Review Series: Lipid droplet synthesis and metabolism: from yeast to man. *J. Lipid Res.* **53**, 215–226.

Chen, X. and Goodman, J.M. (2017) The collaborative work of droplet assembly. *Biochim. Biophys. Acta* **1862**, 1205–1211. https://doi.org/10.1016/j.bbalip.2017.07.003

Ching, S.L., Gidda, S.K., Rochon, A., van Cauwenberghe, O.R., Shelp, B.J. and Mullen, R.T. (2012) Glyoxylate reductase isoform 1 is localized in the cytosol and not peroxisomes in plant cells. *J. Integr. Plant Biol.* **54**, 152–168.

Clark, S.M., Di Leo, R., Dhanoa, P.K., Van Cauwenberghe, O.R., Mullen, R.T. and Shelp, B.J. (2009) Biochemical characterization, mitochondrial localization, expression, and potential functions for an Arabidopsis γ-aminobutyrate transaminase that utilizes both pyruvate and glyoxylate. *J. Exp. Bot.* **60**, 1743–1757.

Clough, S.J. and Bent, A.F. (1998) Floral dip: a simplified method for Agrobacterium-mediated transformation of *Arabidopsis thaliana*. *Plant J.* **16**, 735–743.

Curtis, M.D. and Grossniklaus, U. (2003) A gateway cloning vector set for high-throughput functional analysis of genes *in planta*. *Plant Physiol.* **133**, 462–469.

Davidi, L., Levin, Y., Ben-Dor, S. and Pick, U. (2015) Proteome analysis of cytoplasmatic and plastidic β-carotene lipid droplets in *Dunaliella bardawil*. *Plant Physiol.* **167**, 60–79.

Fan, W., Lam, S.M., Xin, J., Yang, X., Liu, Z., Liu, Y., Wang, Y., Shui, G. and Huang, X. (2017) Drosophila TRF2 and TAF9 regulate lipid droplet size and phospholipid fatty acid composition. *PLoS Genet.* **13**, e1006664.

Fei, W., Shui, G., Zhang, Y. *et al.* (2011) A role for phosphatidic acid in the formation of "supersized" lipid droplets. *PLoS Genet.* **7**, e1002201.

Gao, Q. and Goodman, J.M. (2015) The lipid droplet—a well-connected organelle. *Front. Cell Dev. Biol.* **3**, 49.

Gautier, R., Douguet, D., Antonny, B. and Drin, G. (2008) HELIQUEST: a web server to screen sequences with specific α-helical properties. *Bioinformatics*, **24**, 2101–2102.

Gehl, C., Waadt, R., Kudla, J., Mendel, R.R. and Hänsch, R. (2009) New GATEWAY vectors for high throughput analyses of protein–protein interactions by bimolecular fluorescence complementation. *Mol. Plant*, **2**, 1051–1058.

Gidda, S.K., Shockey, J.M., Falcone, M., Kim, P.K., Rothstein, S.J., Andrews, D.W., Dyer, J.M. and Mullen, R.T. (2011) Hydrophobic-domain-dependent protein–protein interactions mediate the localization of GPAT enzymes to ER subdomains. *Traffic*, **12**, 452–472.

Gidda, S.K., Watt, S.C., Collins-Silva, J. *et al.* (2013) Lipid droplet-associated proteins (LDAPs) are involved in the compartmentalization of lipophilic compounds in plant cells. *Plant Signal. Behav.* **8**, e27141.

Gidda, S.K., Park, S., Pyc, M., Yurchenko, O., Cai, Y., Wu, P., Andrews, D.W., Chapman, K.D., Dyer, J.M. and Mullen, R.T. (2016) Lipid droplet-associated proteins (LDAPs) are required for the dynamic regulation of neutral lipid compartmentation in plant cells. *Plant Physiol.* **170**, 2052–2071.

Goodstein, D.M., Shu, S., Howson, R. *et al.* (2011) Phytozome: a comparative platform for green plant genomics. *Nucleic Acids Res.* **40**(D1), D1178–D1186.

Guo, Y., Walther, T.C., Rao, M., Stuurman, N., Goshima, G., Terayama, K., Wong, J.S., Vale, R.D., Walter, P. and Farese, R.V. Jr (2008) Functional genomic screen reveals genes involved in lipid-droplet formation and utilization. *Nature*, **453**, 657–661.

Hall, T.A. (1999) BioEdit: a user-friendly biological sequence alignment editor and analysis program for Windows 95/98/NT. *Nucleic Acids Symp. Ser.* **41**, 95–98.

Hara, A. and Radin, N.S. (1978) Lipid extraction of tissues with a low-toxicity solvent. *Anal. Biochem.* **90**, 420–426.

Horn, P.J., James, C.N., Gidda, S.K., Kilaru, A., Dyer, J.M., Mullen, R.T., Ohlrogge, J.B. and Chapman, K.D. (2013) Identification of a new class of lipid droplet-associated proteins in plants. *Plant Physiol.* **162**, 1926–1936.

Huang, A.H. (1996) Oleosins and oil bodies in seeds and other organs. *Plant Physiol.* **110**, 1055–1061.

Huang, M.D. and Huang, A.H. (2015) Bioinformatics reveal five lineages of oleosins and the mechanism of lineage evolution related to structure/function from green algae to seed plants. *Plant Physiol.* **169**, 453–470.

Huang, M.D. and Huang, A.H. (2016) Subcellular lipid droplets in vanilla leaf epidermis and avocado mesocarp are coated with oleosins of distinct phylogenic lineages. *Plant Physiol.* **171**, 1867–1878.

Huang, C.Y. and Huang, A.H. (2017) Motifs in oleosin target the cytosolic side of endoplasmic reticulum and budding lipid droplet. *Plant Physiol.* **174**, 2248–2260. https://doi.org/10.1104/pp.17.00366

Ischebeck, T. (2016) Lipids in pollen – They are different. *Biochim. Biophys. Acta* **1861**, 1315–1328.

Kim, H.U., Hsieh, K., Ratnayake, C. and Huang, A.H. (2002) A novel group of oleosins is present inside the pollen of Arabidopsis. *J. Biol. Chem.* **277**, 22677–22684.

Kim, E.Y., Seo, Y.S., Lee, H. and Kim, W.T. (2010) Constitutive expression of CaSRP1, a hot pepper small rubber particle protein homolog, resulted in fast growth and improved drought tolerance in transgenic Arabidopsis plants. *Planta*, **232**, 71–83.

Kim, H.U., Jung, S.J., Lee, K.R., Kim, E.H., Lee, S.M., Roh, K.H. and Kim, J.B. (2013) Ectopic overexpression of castor bean LEAFY COTYLEDON2 (LEC2) in Arabidopsis triggers the expression of genes that encode regulators of seed maturation and oil body proteins in vegetative tissues. *FEBS Open Bio.* **4**, 25–32.

Kim, E.Y., Park, K.Y., Seo, Y.S. and Kim, W.T. (2016) Arabidopsis small rubber particle protein homolog SRPs play dual roles as positive factors for tissue growth and development and in drought stress responses. *Plant Physiol.* **170**, 2494–2510.

Kolkhof, P., Werthebach, M., van de Venn, A., Poschmann, G., Chen, L., Welte, M., Stühler, K. and Beller, M. (2017) A luciferase-fragment complementation assay to detect lipid droplet-associated protein-protein interactions. *Mol. Cell Proteomics*, **16**, 329–345.

Kory, N., Farese, R.V. and Walther, T.C. (2016) Targeting fat: mechanisms of protein localization to lipid droplets. *Trends Cell Biol.* **26**, 535–546.

Krogh, A., Larsson, B., von Heijne, G. and Sonnhammer, E.L. (2001) Predicting transmembrane protein topology with a hidden Markov model: application to complete genomes. *J. Mol. Biol.* **305**, 567–580.

Laibach, N., Post, J., Twyman, R.M., Gronover, C.S. and Prufer, D. (2015) The characteristics and potential applications of structural lipid droplet proteins in plants. *J. Biotechnol.* **201**, 15–27.

Lee, L.Y., Wu, F.H., Hsu, C.T. *et al.* (2012) Screening a cDNA library for protein–protein interactions directly in planta. *Plant Cell*, **24**, 1746–1759.

Li, S., Xu, S., Ma, Y. *et al.* (2016) A Genetic screen for mutants with supersized lipid droplets in *Caenorhabditis elegans*. *G3* **6**, 2407–2419.

Li-Beisson, Y., Shorrosh, B., Beisson, F. *et al.* (2013) Acyl-lipid metabolism. *Arabidopsis Book*, **11**, e0161.

M'barek, K. B., Ajjaji, D., Chorlay, A., Vanni, S., Forêt, L. and Thiam, A.R. (2017) ER Membrane phospholipids and surface tension control cellular lipid droplet formation. *Dev. Cell*, **41**, 591–604.

McCartney, A.W., Greenwood, J.S., Fabian, M.R., White, K.A. and Mullen, R.T. (2005) Localization of the tomato bushy stunt virus replication protein p33 reveals a peroxisome-to-endoplasmic reticulum sorting pathway. *Plant Cell*, **17**, 3513–3531.

McLachlan, D.H., Lan, J., Geilfus, C.M. *et al.* (2016) The breakdown of stored triacylglycerols is required during light-induced stomatal opening. *Curr. Biol.* **26**, 707–712.

Miquel, M., Trigui, G., d'Andréa, S., Kelemen, Z., Baud, S., Berger, A., Deruyffelaere, C., Trubuil, A., Lepiniec, L. and Dubreucq, B. (2014) Specialization of oleosins in oil body dynamics during seed development in Arabidopsis seeds. *Plant Physiol.* **164**, 1866–1878.

Murashige, T. and Skoog, F. (1962) A revised medium for rapid growth and bioassays with tobacco tissue cultures. *Plant Physiol.* **15**, 473–497.

Murphy, D.J. (2012) The dynamic roles of intracellular lipid droplets: from archaea to mammals. *Protoplasma*, **249**, 541–585.

Nelson, B.K., Cai, X. and Nebenführ, A. (2007) A multicolored set of *in vivo* organelle markers for co-localization studies in Arabidopsis and other plants. *Plant J.* **51**, 1126–1136.

Pagac, M., Cooper, D.E., Qi, Y. *et al.* (2016) SEIPIN regulates lipid droplet expansion and adipocyte development by modulating the activity of glycerol-3-phosphate acyltransferase. *Cell Rep.* **17**, 1546–1559.

Page, R.D.M. (1996) TREEVIEW: an application to display phylogenetic trees on personal computers. *Comput. Appl. Biosci.* **12**, 357–358.

Paterson, A.H., Freeling, M., Tang, H. and Wang, X. (2010) Insights from the comparison of plant genome sequences. *Annu. Rev. Plant Biol.* **61**, 349–372.

Petrie, J.R., Shrestha, P., Liu, Q., Mansour, M.P., Wood, C.C., Zhou, X.R., Nichols, P.D., Green, A.G. and Singh, S.P. (2010) Rapid expression of transgenes driven by seed-specific constructs in leaf tissue: DHA production. *Plant Methods*, **6**, 8.

Pol, A., Gross, S.P. and Parton, R.G. (2014) Biogenesis of the multifunctional lipid droplet: lipids, proteins, and sites. *J. Cell Biol.* **204**, 635–646.

Purkrtova, Z., Jolivet, P., Miquel, M. and Chardot, T. (2008) Structure and function of seed lipid-body-associated proteins. *Curr. Rev. Biol.* **331**, 746–754.

Pyc, M., Cai, Y., Greer, M.S., Yurchenko, O., Chapman, K.D., Dyer, J.M. and Mullen, R.T. (2017) Turning over a new leaf in lipid droplet biology. *Trends Plant Sci.* **22**, 596–609.

Rappsilber, J., Mann, M. and Ishihama, Y. (2007) Protocol for micro-purification, enrichment, pre-fractionation and storage of peptides for proteomics using StageTips. *Nat. Protoc.* **2**, 1896–1906.

Richardson, L.G., Howard, A.S., Khuu, N., Gidda, S.K., McCartney, A., Morphy, B.J. and Mullen, R.T. (2011) Protein–protein interaction network and subcellular localization of the *Arabidopsis thaliana* ESCRT machinery. *Front. Plant Sci.* **2**, 20.

Santos Mendoza, M., Dubreucq, B., Miquel, M., Caboche, M. and Lepiniec, L. (2005) LEAFY COTYLEDON 2 activation is sufficient to trigger the accumulation of oil and seed specific mRNAs in Arabidopsis leaves. *FEBS Lett.* **579**, 4666–4670.

Schaab, C., Geiger, T., Stoehr, G., Cox, J. and Mann, M. (2012) Analysis of high accuracy, quantitative proteomics data in the MaxQB database. *Mol. Cell Proteomics*, **11**, M111–014068.

Schmidt, M.A. and Herman, E.M. (2008) Suppression of soybean oleosin produces micro-oil bodies that aggregate into oil body/ER complexes. *Mol. Plant*, **1**, 910–924.

Schmidtt, K., Smolinski, N., Neumann, P., Schmaul, S., Hofer-Pretz, V., Braus, G.H. and Valerius, O. (2017) Asc1p/RACK1 connects ribosomes to eukaryotic phosphosignaling. *Mol. Cell. Biol.* **37**, pii:e00279-16.

Seo, S.G., Kim, J.S., Yang, Y.S., Jun, B.K., Kang, S.W., Lee, G.P., Kim, W., Kim, J.B., Lee, H.U. and Kim, S.H. (2010) Cloning and characterization of the new multiple stress responsible gene I (MuSI) from sweet potato. *Genes Genomics*, **32**, 544–552.

Shevchenko, A., Wilm, M., Vorm, O. and Mann, M. (1996) Mass spectrometric sequencing of proteins silver-stained polyacrylamide gels. *Anal. Chem.* **68**, 850–858.

Shimada, T.L., Shimada, T., Takahashi, H., Fukao, Y. and Hara-Nishimura, I. (2008) A novel role for oleosins in freezing tolerance of oilseeds in *Arabidopsis thaliana*. *Plant J.* **55**, 798–809.

Shimada, T.L., Takano, Y., Shimada, T. *et al.* (2014) Leaf oil body functions as a subcellular factory for the production of a phytoalexin in Arabidopsis. *Plant Physiol.* **164**, 105–118.

Siloto, R.M., Findlay, K., Lopez-Villalobos, A., Yeung, E.C., Nykiforuk, C.L. and Moloney, M.M. (2006) The accumulation of oleosins determines the size of seed oilbodies in Arabidopsis. *Plant Cell*, **18**, 1961–1974.

Sim, M.M., Dennis, R.J., Aubry, E.M., Ramanathan, N., Sembongi, H., Saudek, V., Siniossoglou, S. and Rochford, J.J. (2013) The human lipodystrophy protein seipin is an ER membrane adaptor for the adipogenic PA phosphatase lipin 1. *Mol. Metab.* **2**, 38–46.

Stefano, G., Renna, L. and Brandizzi, F. (2015) BiFC for protein–protein interactions and protein topology: discussing an integrative approach for an old technique. *Methods Mol. Biol.* **1242**, 173–182.

Talukder, M.M.U., Sim, M.M., O'Rahilly, S., Edwardson, J.M. and Rochford, J.J. (2015) Seipin oligomers can interact directly with AGPAT2 and lipin 1, physically scaffolding critical regulators of adipogenesis. *Mol. Metab.* **4**, 199–209.

Theodoulou, F.L. and Eastmond, P.J. (2012) Seed storage oil catabolism: a story of give and take. *Curr. Opin. Plant Biol.* **15**, 322–328.

Thiam, A.R. and Beller, M. (2017) The why, when and how of lipid droplet diversity. *J. Cell Sci.* **130**, 315–324.

Thiam, A.R. and Forêt, L. (2016) The physics of lipid droplet nucleation, growth and budding. *Biochim. Biophys. Acta* **1861**, 715–722.

Thiam, A.R., Farese, R.V. Jr and Walther, T.C. (2013) The biophysics and cell biology of lipid droplets. *Nat. Rev. Mol. Cell Biol.* **14**, 775–786.

Tsai, C.H., Zienkiewicz, K., Amstutz, C.L., Brink, B.G., Warakanont, J., Roston, R. and Benning, C. (2015) Dynamics of protein and polar lipid recruitment during lipid droplet assembly in *Chlamydomonas reinhardtii*. *Plant J.* **83**, 650–660.

Vanhercke, T., Divi, U.K., El Tahchy, A. *et al.* (2017) Step changes in leaf oil accumulation via iterative metabolic engineering. *Metab. Eng.* **39**, 237–246.

Viljoen, A., Dubois, V., Girard-Misguich, F., Blaise, M., Herrmann, J.L. and Kremer, L. (2017) The diverse family of MmpL transporters in mycobacteria: from regulation to antimicrobial developments. *Mol. Microbiol.* **104**, 889–904.

Vizcaíno, J.A., Csordas, A., del-Toro, N. *et al.* (2016) 2016 update of the PRIDE database and its related tools. *Nucleic Acids Res.* **44**, 11033.

Walter, P. and Johnson, A.E. (1994) Signal sequence recognition and protein targeting to the endoplasmic reticulum membrane. *Annu. Rev. Cell Biol.* **10**, 87–119.

Welte, M.A. and Gould, A.P. (2017) Lipid droplet functions beyond energy storage. *Biochim. Biophys. Acta* **1862**, 1260–1272. https://doi.org/10.1016/j.bbalip.2017.07.006

Xing, S., Wallmeroth, N., Berendzen, K.W. and Grefen, C. (2016) Techniques for the analysis of protein-protein interactions in vivo. *Plant Physiol.* **171**, 727–758.

Yang, H.J., Hsu, C.L., Yang, J.Y. and Yang, W.Y. (2012) Monodansylpentane as a blue-fluorescent lipid-droplet marker for multi-color live-cell imaging. *PLoS ONE*, **7**, e32693.

Yu, S., Viswakarma, N., Batra, S.K., Rao, M.S. and Reddy, J.K. (2004) Identification of promethin and PGLP as two novel up-regulated genes in PPARγ1-induced adipogenic mouse liver. *Biochimie*, **86**, 743–761.

Zacharias, D.A., Violin, J.D., Newton, A.C. and Tsien, R.Y. (2002) Partitioning of lipid-modified monomeric GFPs into membrane microdomains of live cells. *Science*, **296**, 913–916.

Zhang, Z., Cheng, Z.J., Gan, L. *et al.* (2016) OsHSD1, a hydroxysteroid dehydrogenase, is involved in cuticle formation and lipid homeostasis in rice. *Plant Sci.* **249**, 35–45.

